Journal of Hydrology: Regional Studies 41 (2022) 101072

Contents lists available at ScienceDirect

Journal of Hydrology: Regional Studies

journal homepage: www.elsevier.com/locate/ejrh

Land use and land cover change and its impact on river morphology in Johor River Basin, Malaysia

Chuen Siang Kang [a], Kasturi Devi Kanniah [a,b,*]

[a] Faculty of Built Environment and Surveying, Universiti Teknologi Malaysia, 81310 Johor Bahru, Johor, Malaysia
[b] Centre for Environmental Sustainability and Water Security (IPASA), Research Institute for Sustainable Environment (RISE), Universiti Teknologi Malaysia, 81310 Johor Bahru, Johor, Malaysia

ARTICLE INFO

Keywords:
Land Use Land Cover (LULC) change
Google Earth Engine (GEE)
Johor River Basin
River Morphology
Channel migration

ABSTRACT

Study Region Johor River Basin (JRB), Malaysia. Study Focus The study generates long time-series land use and land cover (LULC) change at 5- years interval using Google Earth Engine and investigate the LULC changes and river morphology changes of JRB. Intensity analysis on the LULC changes was conducted to highlight the transition between LULC. Targeted transition from natural to disturbed lands were detected, which impact the river morphology of the basin. River morphology changes were identified along Johor River, based on the centerline migration derived from Channel Migration Toolbox. New Hydrological Insights for the Region JRB has undergone high intensity LULC change over the past decades due to significant economic and population growth which impacted the river morphology. Channel migration analysis reported high river centerline migration (498609 m^2 to 1853886 m^2) of Johor River. Higher migration rate was identified at the estuary of the Johor River and several locations along the river. Specific locations with high channel migration were highlighted where human-induced changes are the factors to affect the morphology of the river. The proposed method is first applied in the region and the results enhance local and regional policies and decision making on food and water security, prevent extreme events such as floods, and further degradation of natural land.

1. Introduction

Over the past decades, one-third of the global land use has been changed either once or on multiple occasions (Winkler et al., 2021). The dynamicity of Land Use and Land Cover (LULC) change has triggered issues related to environmental, ecosystem, water, food security, climate change, etc. (Song et al., 2018; Winkler et al., 2021). The LULC science includes characterization of land cover and land use and quantification of their changes and their consequences. Drivers of these changes are either natural, such as climate variability and change, or anthropogenic, such as socio-economic or political (Roy and Roy, 2010). Any human-induced landscape modification driven by economy or politics has impacts on major components in the Earth system, such as carbon cycle, surface hydrology, and atmospheric processes (Zhao et al., 2006). These changes also affect social systems and impact food security, energy production, and water resources (Wolde et al., 2021).

Water is the foundation to sustain life (Guppy and Anderson, 2017). Half of the world's population reside at the vicinity of river (< 3 km) to obtain their main source of water (freshwater) supply (Kummu et al., 2011); and daily essentials such as economic activities,

* Corresponding author at: Faculty of Built Environment and Surveying, Universiti Teknologi Malaysia, 81310 Johor Bahru, Johor, Malaysia.
E-mail address: kasturi@utm.my (K.D. Kanniah).

https://doi.org/10.1016/j.ejrh.2022.101072
Received 2 September 2021; Received in revised form 9 February 2022; Accepted 30 March 2022
Available online 7 April 2022

transportation, and natural resources exploration (Fang et al., 2018). However, water scarcity and security issues have emerged at national and global scales due to rapid population growth. By 2050, more than 40% of the world's population will get their daily water supply from water-stressed river basins (OECD, 2001). This increase of supply-and-demand of water and resources relative to the global population growth has led to significant LULC change especially at the vicinity of rivers, which can severely impact the river physical characteristics and ecology (Chin, 2006; Zhao et al., 2006). How LULC changes impact a river basin from various perspectives have been studied (Chin, 2006), including runoff and water availability (Wang et al., 2017), discharge (Petchprayoon et al., 2010), water yield (Geng et al., 2015), headwater fluvial (Harden, 2006), morphology and structure (Kudnar, 2020; Yousefi et al., 2019) and dam construction (WWF, 2004). River morphology refers to the shape of river channels and identifying their changes in terms of the area/zone and direction (channel migration) over time can help communities residing near the river bank to guide development away from channel migration zones and reduce flood hazards.

Recent studies by Kong et al. (2020) and Ibitoye (2021) proved that the natural and anthropogenic activities are the main cause of river morphology changes. The Johor River Basin (JRB) located in the southern state of Peninsular Malaysia has an important role to supply water for local usage and to support part of the water demand of Singapore (Chuah et al., 2018). It is in a humid tropical region with monsoon seasons and is occasionally influenced by El Nino events and severely impacted by floods for the past decades (Kia et al., 2012; Saudi et al., 2015). Droughts, floods, dams and barrage construction, and land reclamation within or surrounding the basin can severely affect the naturality of the basin. Thus, it has become a popular area for research particularly relating to hydro-climatology studies including floods (Ismail et al., 2015), streamflow (Tan et al., 2015), runoff (Dorofki et al., 2012), drought (Tan et al., 2019a, 2019b), and soil erosion (Obaid and Shahid, 2017) which are impacted by the LULC changes over the years under the rapid development of the area. Wang et al. (2019) identified several land sprawl construction and land reclamation areas over the southern part of the JRB, particularly at Tekong Island, Singapore, to accommodate the economic development and inhabitants surrounding the river basin. This indicates that the JRB and its surrounding area are rapidly changing, which could have a direct impact on the hydrology and ecology of the river basin. In addition, anthropogenic activities including construction of dams and barrage along the JRB have affected the natural stability of the river basin, although these activities were to ensure water security and prevent floods in the area (Lin, 2011).

Studies investigating the impact of LULC changes on river morphology are limited and only a few researchers have been conducted to date in Portugal (Fernandes et al., 2020), India (Himayoun and Roshni, 2020), Iran (Yousefi et al., 2019, 2016), Nigeria (Ibitoye, 2021). Despite being a popular study site due to its importance to the region, a long-term analysis on LULC changes within the JRB and the impacts on the river morphology is yet to be conducted (Awang Ali et al., 2017). LULC classification and change detection over the tropical region is always a painstaking task due to the lack of multi-temporal cloudless satellite data and insufficient ground sampling. To date, most of the LULC classification or change detection studies conducted in tropical region are based on satellite images contains with some clouds and cloud shadows (Deilmai et al., 2014; Kanniah et al., 2021, 2016, 2015; Tan et al., 2010). Intensity analysis of LULC has been successfully applied globally to improve the understanding of the transition between various land use classes (Ekumah et al., 2020; Estoque and Murayama, 2015; Gandharum et al., 2022; Yang et al., 2017; Zhou et al., 2014). This advanced analytical technique is also useful on detecting errors on historical classification maps which ground truth samples are usually unavailable (Enaruvbe and Pontius, 2015; Sun et al., 2021; Tankpa et al., 2020), and added advantage to explain the LULC results in a more detailed manner. Moreover, although LULC classification is a popular research in Malaysia, no previous studies applied intensity analysis to describe LULC changes in Malaysia. This study utilized the Google Earth Engine (GEE), a cloud-based platform featuring big data processing, using a collection of publicly available remote sensing imagery and products (Gorelick et al., 2017) for LULC classification. Although the GEE has gained much publicity, a review by Amani et al. (2020) summarized machine learning and land cover as being a popular research area based on GEE, only a few studies have been conducted in Malaysia over the years. Shaharum et al. (2020) compared SVM, RF, and Classification and Regression Tree (CART) classifiers to classify oil palm in Malaysia on 2016–2017 using Landsat 8 data. Wahap and Shafri (2020) also compared these three classifiers over Klang valley area for year 1998, 2003 and 2018. Ju et al. (2021) combines Landsat 8 and Sentinel-2 images with a number of indices to perform land classification of JRB but only focused on year 2019. To our knowledge, there are limited studies conducted on JRB to identify the impacts of LULC changes to the dynamics of river morphology over a long period. The impacts of LULC changes within the river basin can support future planning, management, and sustainable development of the JRB and its surrounding areas, it will also assist further studies involving ecosystem conservation and services, sustainable land use planning, natural disaster (floods) prevention and water security.

This study aims to analyze the impacts of LULC changes within the JRB to the Johor river morphology over the past 30 years based on remote sensing and geographic information science (GIS) techniques. More specifically, two machine learning algorithms were compared to delineate different land use and land cover classes. The intensity of the LULC changes was then analysed at 5 years' intervals between 1990 and 2020. River features classified from the satellite images were processed to generate river centerlines and migration polygons. A detailed analysis on river morphology was performed on locations that underwent significant changes over time. The results from this study will support the local understanding on the LULC changes and the impact to the river morphology of the JRB. It will provide useful data to inform local and national policies and development plans that will contribute to the United Nations' Sustainable Development Goals (UN SDGs) for sustainable development and climate change, i.e., SDG 11 and SDG 13.

2. Study area

Over the past three decades, Malaysia's population grew from 18.4 million to 32.7 million (mean annual growth of 2.0%). The state of Johor is strategically located between the Straits of Melaka at its west, South China Sea at its east, and Singapore at its south, and has become one of the focused regions for urbanization and economic development in Malaysia. As the development offers opportunities,

Johor recorded a higher population growth rate of 2.6% (2.1 million to 3.7 million) than the national rate over the same period (Department of Statistics Malaysia, https://www.dosm.gov.my, accessed on 7th July 2021).

The Johor River Basin (1.426–2.080 N and 103.330 E to 104.075 E) is located in the state of Johor at the southern part of Peninsular Malaysia. The ecosystem services of the JRB, particularly on water supply, makes it one of the most highlighted basins in the area. The JRB supplies water to the southern Johor zone (where the capital city of Johor Bahru is located) and to Singapore. The JRB is distributed over 4 districts in Johor, namely Kluang, Johor Bahru, Kota Tinggi and Mersing, where the Johor River is the main river with a total length of 122 km. Originating from Mount Belumut (1010 m) at the northern part of the basin, its major tributaries include the Linggui, Sayong, Tiram, and Seluyut Rivers (Fig. 1(b)). The whole of the JRB considered in this study covers an area of about 238600 ha . Part of it is within the Iskandar Malaysia zone which has been the focus development area of Malaysia since 2006. Land transformation due to urbanization, dam constructions and agricultural activities, have been some of the major LULC changes in the JRB over the decades, to cope with the increased population, water demand and to support economical income from industrial and agricultural sectors. Fig. 1(a) and (b) show the location of the JRB in the Johor state of Peninsular Malaysia.

3. Data and methodology

The methodology of this study is divided into two parts. The first part involves digital image classification of cloudless Landsat image composites that were generated using GEE based on two machine learning classifiers, the accuracy assessment and change detection analysis, and the LULC change intensity analysis. The second part involves the analysis on the river morphology changes using the Channel Migration Toolbox (CMT) over the study period in JHB. Fig. 2 shows the general workflow of the study, and the following subsections describes the procedures in detail.

3.1. Google Earth Engine

The Google Earth Engine (GEE) is a user-friendly, open source, web-based cloud computing platform featuring big-geodata access, processing, interpretation, and analysis (Amani et al., 2020). Since the introduction of the GEE in 2010, multiple satellites data collection is made available including from the Landsat mission, which is the most widely used dataset (Kumar and Mutanga, 2018) with a collection covering around 40 years since the 1970 s (Tamiminia et al., 2020). Recent studies utilized GEE to generate Landsat time-series LULC changes analysis and comparing different classification techniques over variety of study sites, benefiting from the vast data availability and fast computing capability of GEE (Brovelli et al., 2020; Nyland et al., 2018; Richards and Belcher, 2020; Shaharum et al., 2020; Xie et al., 2019). These studies suggest that GEE could accelerate and improve the long time-series LULC classification over selected area or regions. The GEE was applied in this study to produce Landsat image composites at 5 years gap, and to perform machine learning classification and confusion matrix analysis. Operating on a cloud-based platform, the computing power of the GEE facilitates data collection, classification, and analysis processes at a very fast speed. The following sections describe the detailed methodology used in the GEE to achieve accurate LULC classification maps for the JRB.

3.1.1. Cloudless Landsat image composite

Landsat is one of the satellite datasets in the GEE image collections. Although the first Landsat satellite was launched in 1972, a

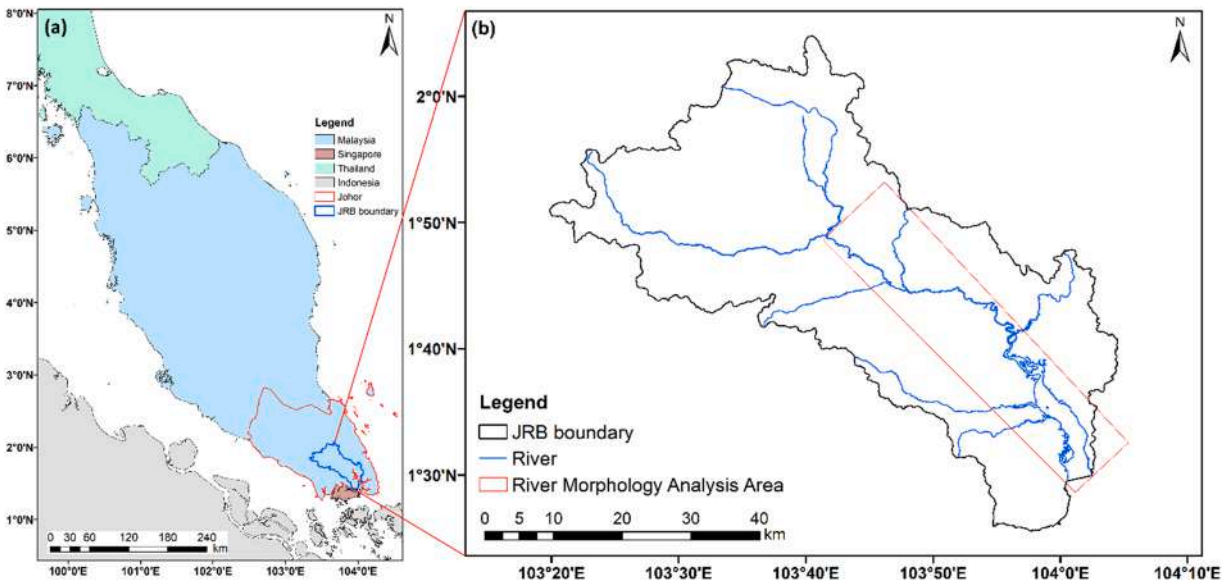

Fig. 1. Location of the JRB in Peninsular Malaysia (a) and the rivers in the basin (b).

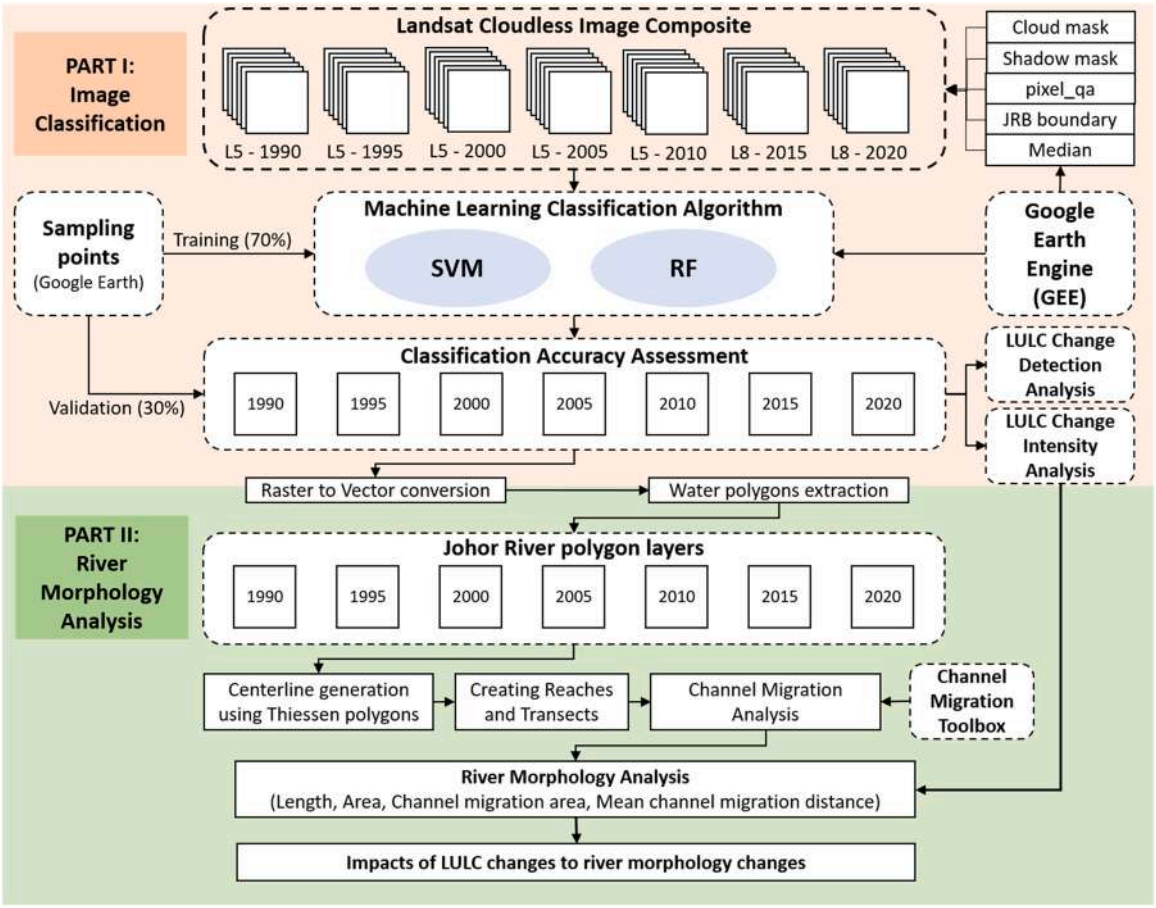

Fig. 2. Workflow chart describing the methodology of the study.

complete coverage of the Landsat image composite over the study area is only available from 1990. Therefore, Landsat-5 Thematic Mapper (TM) and Landsat-8 Operation Land Imager (OLI) were used to generate the image composites (at 5 years interval) for classification purposes. The Landsat collection of Tier 1 Surface Reflectance (T1_SR) which underwent atmospheric correction including cloud, shadow, water, and snow mask processes, was selected in this study. Both Landsat 6 (failed to enter the orbit) and Landsat 7 (scan line corrector failure) were left out from the selection. Table 1 summarizes the characteristics of Landsat 5 and Landsat

Table 1
Landsat-5 and Landsat-8 sensors' characteristics. Bands in *Italics* were excluded from the classification due to different spatial resolution.

Satellite	Band	Wavelength (μm)	Resolution (m)
Landsat-5 Thematic Mapper	1 – Visible Blue	0.45 – 0.52	30
	2 – Visible Green	0.52 – 0.60	30
	3 – Visible Red	0.63 – 0.69	30
	4 – Near-Infrared	0.76 – 0.90	30
	5 – Near-Infrared	1.55 – 1.75	30
	6 – Thermal	*10.40 – 12.50*	*120*
	7 – Mid-Infrared	2.08 – 2.35	30
Landsat-8 Operation Land Imager	1 – Coastal Blue	0.43 – 0.45	30
	2 – Visible Blue	0.45 – 0.51	30
	3 – Visible Green	0.53 – 0.59	30
	4 – Visible Red	0.64 – 0.67	30
	5 – Near-Infrared	0.85 – 0.88	30
	6 – Shortwave Infrared (SWIR) 1	1.57 – 1.65	30
	7 – Shortwave Infrared (SWIR) 2	2.11 – 2.29	30
	8 – Panchromatic	*0.50 – 0.68*	*15*
	9 – Cirrus	1.36 – 1.38	30
Thermal Infrared Sensor	*10 – Thermal Infrared (TIRS) 1*	*10.60 – 11.19*	*100*
	11 – Thermal Infrared (TIRS) 2	*11.50 – 12.51*	*100*

8 sensors.

Cloud cover is always an issue for optical remote sensing images acquired over the equatorial region. To overcome this issue, a cloud masking function was applied during the image composition process. The bitmask for pixel_qa (pixel quality attributes) bands were considered to mask the clouds and cloud shadow on each Landsat image within each period of interest. Table 2 lists the detail of the periods and number of scenes used to generate each image composite. The default period to generate the image composite is one year, while for several cases, there are still some masked pixels found on the image composite. Thus, a longer timeframe was set to overcome this issue. For example, a timeframe of 2 years (01/01/2004–31/12/2005) was set to generate the image composite for year 2005. Based on local knowledge, we assume that there are no massive land use and land cover change occurred during the 2 years interval within the 5 years window considered in this study. This assumption is supported by 1) the transition from forest to agriculture or urban requires land clearance which normally takes years to complete, 2) the built-up of residential and commercial buildings from bare soil requires at least 3 years to complete, 3) the clearance and replanting of crops in the study area can be completed within 2–3 years period. Therefore, we believe that 5 years interval set in this study could be appropriate and representable to the actual land use land cover changes.

Once the Landsat images were listed from each timeframe, the median of each pixel in the JRB was computed to create the cloudless Landsat scenes within each timeframe. Median reduction method is used in this study because it is a promising technique in GEE to process image composite which can provide equal or improved classification accuracy when compared to other reduction method (mean, minimum, maximum, percentile, etc.), single-image and timeseries images (Feizizadeh et al., 2021; Nyland et al., 2018; Phan et al., 2020; Richards and Belcher, 2020; Xie et al., 2019). Li et al. (2019) and Luo et al. (2022) proved that the median image composite method based on multi-year images could minimize the impact of extreme outliers caused by the seasonal and weather effects, resulting a robust image composite for mapping. Therefore, the cloudless Landsat image composites generated based on the above procedures are assumed to have stable spectral characteristics and minimal seasonal effects, where the changes of water level and river wetted cross-sections will not significantly impact the classification, extraction of river polygons and its centerlines, as well as the river morphology analysis. Fig. S1 shows the true color cloudless Landsat image composite of each time interval.

3.1.2. Machine learning classification

Machine learning classification is one of the most applied functions in GEE, which includes both supervised and unsupervised algorithms (Amani et al., 2020). This study utilized support vector machine (SVM) and Random Forest (RF) classifiers available on GEE platform (Gorelick et al., 2017). Based on two recent reviews by Tamiminia et al. (2020) and Sheykhmousa et al. (2020), both SVM and RF can provide comparable high accuracy. While both support vector machine (SVM) and random forest (RF) are the most selected machine learning classifier over the recent years (Sheykhmousa et al., 2020), conclusion on which classifier performs better in LULC classification is not clear. Thus, this study compared the two classifiers and analysed their capability in terms of classification accuracy and visual appearance.

3.1.2.1. Support vector machine classifier. A SVM classifier based on the supervised non-parametric statistical learning technique separates the data into classes by optimization of separation hyperplanes. SVM was first introduced in the late 1970 s and the strength of SVM is its ability to solve the local extremum dilemma present in the machine learning techniques, by obtaining a global optimal solution by solving the convex quadratic optimization problem. The optimization is generally defined by applying soft margin or kernel functions (polynomial, radial basis, gaussian radial basis, sigmoid) to solve inseparability issues caused by mixing effects which is common in remote sensing image classification. In addition, SVM requires only small training sets to produce higher accuracy than a traditional classifier, however, it has shortcomings when dealing with noisy data (Mountrakis et al., 2011; Tamiminia et al., 2020).

3.1.2.2. Random forest classifier. Random Forest (RF) is the most popularly applied machine learning classifier (Belgiu and Drăguţ, 2016) and the most frequently used classifier on the GEE platform (Tamiminia et al., 2020). RF, which is based on the decision tree method with an ensemble learning approach, utilizes boosting and bagging procedures to solve the classification of satellite image pixels. The boosting technique integrates multiple models to solve the same problem, hence increasing the classification accuracy. The accuracy of RF classification relies on two parameters, namely the number of trees (*Ntree*) and number of features (*Mtry*). The classification accuracy of RF is more sensitive to *Mtry* than *Ntree*, where a smaller *Mtry* would shorten the processing time but provides

Table 2
Details of periods and number of scenes applied to generate each image composite.

Satellite	Year	Timeframe		n
		Start	End	
Landsat-5	1990	1989/06/01	1990/12/31	34
	1995	1994/06/01	1996/05/31	76
	2000	1999/06/01	2001/05/31	78
	2005	2004/01/01	2005/12/31	87
	2010	2009/01/01	2010/12/31	61
Landsat-8	2015	2014/09/01	2015/12/31	67
	2020	2020/01/01	2020/12/31	53

*n = number of scenes compiled.

lower accuracy. It is common to set *Ntree* as large as possible as this will not affect the efficiency and cause over fitting during the classification process (Belgiu and Drăguţ, 2016).

3.2. LULC class descriptions

This study classifies a total of six LULC classes. LULC classes based on the local landuse map provided by the National Land Use Information Division, Department of Town and Country Planning Malaysia was referred and simplified. Water class in this study includes rivers, ponds, and dams in the study area. Forest class refers to the inland forest while Mangrove class refers to wetland forest located by the river or shorelines. Agricultural class includes oil palm plantation, rubber plantation, and other agricultural lands. The commercial, industrial, residential, infrastructure and utilities, and transportation (road networks) are classified as Urban. Bare soil includes empty lands and cleared lands where the soil surface can be detected from the images.

3.3. Sampling points

Lack of field-based data collection is always an issue when conducting a long-term LULC analysis. In this study, on-screen selection of sample points from high-resolution Google Earth images were conducted to provide the training and validation points. This method is theoretically proven and practiced in Kanniah (2017); Lin et al. (2018). During the selection of the sample points, the time-slider function of Google Earth was used to ensure the data used to select the sample points were within the specific period of interest according to Table 2. For all the periods, 300 points were randomly identified and the portion of the points for each land use class were roughly distributed based on the area of each class. For example, (1) agriculture is the major land use in the JRB, thus the majority sample points selected are for agriculture (almost half of the total sample points), and (2) the sample points for water on year 1990 is 50, while we increased the number of points to 60 after year 1995 since there were more water bodies found in the study area. In order to reduce the impact of the location of the sample points to the classification results, we tried to maintain most of the sample points at the same location throughout the 30 years' study period, unless land use change was identified visually during the sample point selection. The selected sample points were imported to GEE script to run the classification. During the classification process, the sample points were randomly divided into 2 categories, namely training sample (70%) and validation samples (30%).

3.4. Post-classification and accuracy assessment

A minimum mapping unit (MMU) was applied at post-classification to improve the quality of the classified maps. A window size of 3×3 was used on each classified map to generalize spurious pixels according to the neighboring pixels. This process can remove noise and salt-pepper effects from the output maps. The GEE platform also supports classification analysis including the confusion matrix which is also used to compute the overall accuracy (OA), producer accuracy (PA), consumer accuracy (CA) and Kappa coefficient (KC). OA is the ratio between the sum of the major diagonal to the total number of sample points. PA and CA are two accuracy parameters to show the agreement between the sample points to a specific class, from the perspective of the producer or the consumer, respectively. PA is computed by dividing the major diagonal value of the class (samples that are correctly classified) to the sum of the samples for that class. CA is computed by dividing the major diagonal value by the total number of sample classified/mapped as that class. Finally, the KC was computed for each classification map to test whether the result is significantly better than a random classification. A KC above 0 also refers to significant agreement between the classification map with the reference sample points (Congalton and Green, 2019). Thus, the OA, PA, CA, and KC were reported in this study for both the SVM and RF classification map of every selected period.

3.5. LULC changes analysis

Located within the rapidly developing state of Malaysia, JRB has been subject to intense analysis on the LULC changes to show how and what are the major land uses that have changed over the study period. Besides comparison on the total area and percentage of each LULC class, change detection analysis is normally conducted to detect the area changes from one class to another. A matrix with computed pixel counts or area of the changes was produced from the change detection of two periods, and maps were generated to visually identify the area of significant changes.

In order to understand the LULC changes in more detail, an advance analysis method such as intensity analysis was introduced by Aldwaik and Pontius (2012) and tested on several sites including Plum Island in Boston, Zhenlai County in China (Yang et al., 2017), and two developing cities in Southeast Asia – Bangkok and Manila (Estoque and Murayama, 2015). Intensity analysis of LULC changes can be performed based on the data derived from the change detection matrix. Intensity analysis can be divided into three levels, which are interval intensity, category intensity and transition intensity. The interval intensity compares the uniform intensity calculated as the rate of change of the whole study period to the rate of change of each time interval. The annual rate of changes also can be computed by dividing the interval rates to the number of years of each period. By comparing the annual intensity rate to the uniform intensity rate, the LULC change of a specific area can be identified as slow- or fast-paced over a specific period. The category intensity computes the annual change intensity of each category based on the gross gains and gross losses, then the intensity is compared to the uniform intensity. This comparison examines which category actively changes or stays dormant over the period. The transition intensity explaining the gains (or losses) of a particular category are targeted from (or avoided from) which category. It can highlight how intensely a category changed from (or to) another category. The equations involved in computing the interval, category and transition intensities can be referred to in Aldwaik and Pontius (2012). Hypothetical errors of each time interval were calculated to

explain the deviation of each classification map from the uniform transitions as shown in Enaruvbe and Pontius (2015), with consideration of classification errors may influence the accuracy of the intensity analysis.

3.6. River morphology changes

To investigate the morphological changes (channel migration) of the Johor River, the raster classification maps of the JRB were vectorized, and the polygons of water bodies (rivers, dams, ponds, etc.) were extracted. At a 30-meter spatial resolution of Landsat composite images, some parts of the river and tributes with width less than the Landsat spatial resolution are not clearly identified due to the mixing pixel effects commonly occurring in remote sensing data. Therefore, we limited the river morphology analysis to the main river (Johor River) in the JRB (Fig. 1(b)). Fig. 3 describes the steps applied to derive river centerlines and use the centerlines to compute river migration area and distance. Firstly, the area of the Johor River was computed based on the polygons and compared among the different years to understand the areal changes of the river over time. Secondly, the centerlines of the river were generated from the river polygons (Fig. 3(a & b)) using the *Create Thiessen Polygon* function in ArcGIS version 10.5 (Lewandowicz and Flisek, 2020). Centerlines are commonly used to investigate the morphological changes of a river (Ibitoye, 2021; Kong et al., 2020). During this process, the centerlines were generated based on the boundary of the polygons, so the centerlines can represent the changes of the shape and direction (morphology) of the river. The length of the centerlines was then compared among the years to define the changes of the total length of Johor River over the period.

The Channel Migration Toolbox (CMT) (Legg et al., 2014) developed by the Department of Ecology, State of Washington, USA, integrated in ArcGIS 10.5 was used to analyse the morphological changes. The main purpose of CMT is to measure river migration rates along the entire river and within the river reaches (sections of the river). Transects were drawn within the reaches to directly measure river migration at specific locations (Fig. 3(c & d)) (Legg et al., 2014). Three tools were used in the CMT to derive the migration area/zone and distance of the river, namely: 1) Reach-Average Channel Migration Tool, 2) Transect Generation Tool, and 3) Transect Channel Migration Tool. By importing the river centerlines into the CMT, the first tool overlays the centerlines to create polygons that represent the migration area/zone during each specific period. In order to analyse the river changes in a more detailed manner, 13 reaches at different lengths were set along the river (R-1 to R-13, Table 3). The function of these reaches is to separate the entire river

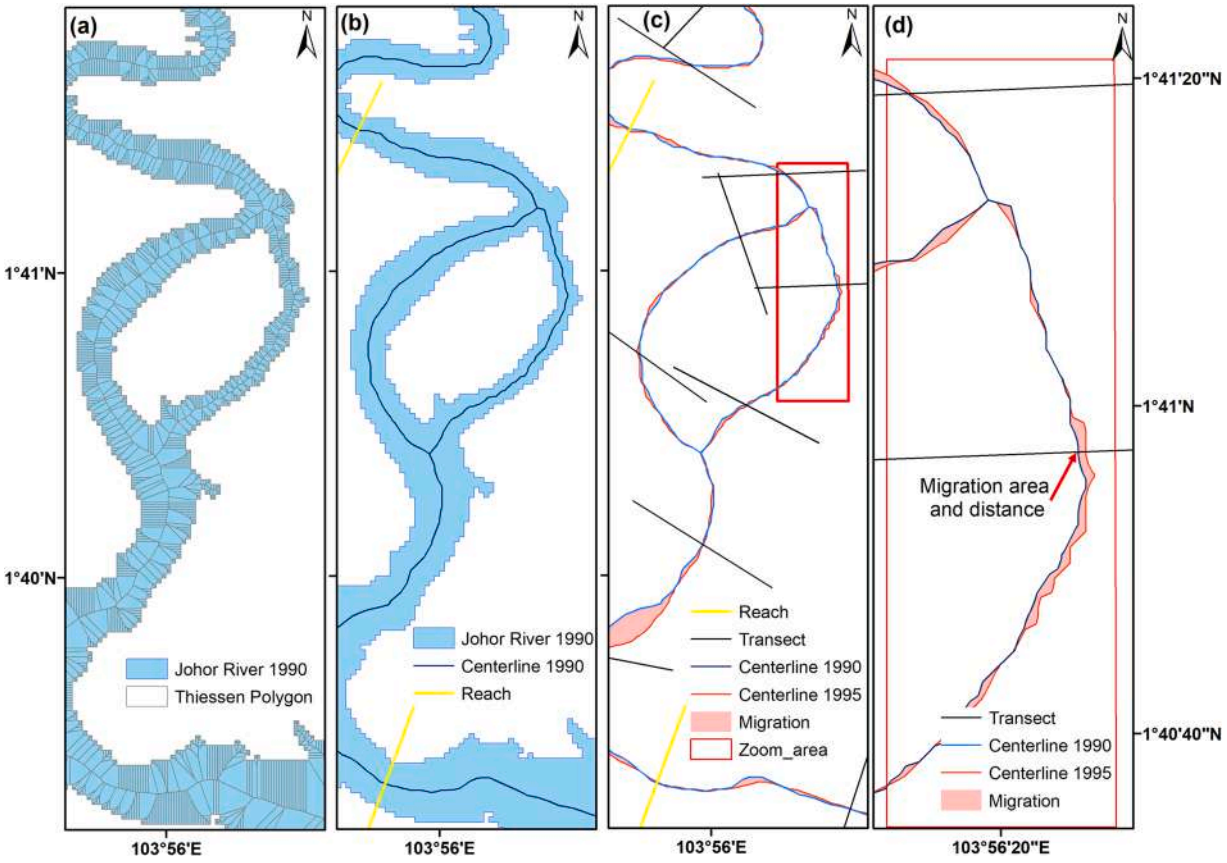

Fig. 3. Methodology applied to create Thiessen polygons within the river polygon (a), river centerline and reaches (b), transects and channel migration areas and distance using centerlines (c), and polygons showing the migrated area and how the transects are overlayed to derive the migrated distance (d).

into sections, so the migration rate of each reach can be clearly defined and analysed. The second tool generates the transects within each reach at a user-specified gap. The distance between transects is relative to the width of the river, where greater transect gap is recommended for wider river (Legg et al., 2014), thus different number of transacts were generated for each reach considering the relative width of the river. Table 3 summarizes the gap set for the transects and the number of transects within each reach. The third tool applied in this study overlays the transects on to the migration area polygons defined from Tool 1. The lateral movements of centerlines across multiple periods can be measured using this tool, and the distance of the migration at each transects are exported. Based on the transects migration distance table, analysis such as the migration distance of specific transects, mean migration distance within each reach, and total migration distance of the entire river can be computed. Analysis of the impact of LULC changes on river morphology changes was performed by comparing the LULC change intensity with the total migration area and total migration distance computed from CMT. Furthermore, specific locations with significant river migration were highlighted and the reasons for the river morphology change were discussed.

4. Results and analysis

4.1. Classification maps and accuracy assessment

Classification procedures based on GEE minimize the time and steps required to complete the classification of the JRB over three decades with 5 years interval. Classification maps for years 1990, 1995, 2000, 2005, 2010, 2015, and 2020 were produced based on the cloudless Landsat image composites (described in Section 3.1.1). Table 4 lists the PA, CA, OA, and KC for each year and their respective classes. Statistically, the RF classifier has higher OA and KC when compared to the SVM classifier. Both SVM and RF classifiers showed very high accuracy above 0.90 and RF recorded perfect classification accuracy on several occasions (OA = 1.00). According to Breiman (2001), it is possible for RF classifier to produce OA of 1.0 due to several reasons when: (1) the RF has built a full grown tree, and (2) RF is based on the bootstrapped training sets that the out-of-bag method decreases the error rate. In addition of the high accuracy of SVM and RF, the spatial distribution of the classification maps generated from SVM (Fig. 4), and RF (Fig. S2) are also similar. However, from detail visual interpretation on the output maps, we found that the SVM classifier performed better on identifying narrow river, when compared to the results from the RF classification. The rivers identified using the SVM classifier were found to be mis-classified as their surrounding land use classes in the RF classifier. Fig. 5 shows a zoomed location comparing this issue. From Fig. 5, we can notice that the Sayong river located at the western side of the Johor River Basin was correctly classified using the SVM classifier but some parts of the Sayong river were classified as Agricultural area when the RF classifier was applied. Based on this finding, we conclude that despite the RF classifier produced a higher classification accuracy, it can only produce more generalized classification maps. The SVM classifier on the other hand is found to capture more details, especially over narrower features such as rivers in the JRB region. This finding is corresponded to Zagajewski et al. (2021) who found that SVM has superiority on classifying heterogeneous area, capture more features, and detecting edge pixels (Heydari and Mountrakis, 2018), while RF tends to be more generalized on agricultural area (Dabija et al., 2021). The potential of the RF classifier to delineate narrow features needs to be explored further. Therefore, in the following section the results produced from the SVM classification are described and discussed.

Fig. 4 shows the majority of the LULC of the JRB is for agricultural usage with agricultural land covering more than 60% (150000 ha) of the basin in all the years analyzed in this study. This is followed by forest land that covers about 20% of the basin. Most of the forests are found at the northeastern part of the basin and other forest patches are located at the middle and the eastern part of the basin. Urban development is found to be expanding at the southern part of the basin while mangroves are located along the Johor River and its estuary. This type of LULC distribution is common in the SEA region where the majority of forest lands were cleared for agricultural crops, and urbanization surrounding the river (Kummu et al., 2011) being the main water source for daily supply and industrial usage. The construction of dams became a common practice in SEA as well as at global scale, primarily at the area of rapid population growth (Sabater et al., 2018), such as in the JRB.

Table 3
Reaches and transects of the Johor River Basin generated for the channel migration analysis.

Reach	Reach Length (m)	Transect gap (m)	No. of Transects
R-1	5000.00	500	10
R-2	5000.00	500	10
R-3	5000.00	500	10
R-4	5000.00	500	10
R-5	5000.00	750	7
R-6	5000.00	750	7
R-7	5000.00	750	7
R-8	5000.00	750	7
R-9	5000.00	1000	5
R-10	8000.00	1000	8
R-11	12309.59	1500	8
R-12	9000.00	1500	6
R-13	15619.18	1500	10

Table 4
The Producer accuracy (PA), Consumer accuracy (CA), Overall accuracy and Kappa values of the classification results.

Year	Classifier	Water		Urban		Agricultural		Forest		Mangrove		Bare soil		Overall	Kappa
		PA	CA	PA	CA	PA	CA	PA	CA	PA	CA	PA	CA	accuracy	coefficient
1990	**SVM**	**0.973**	**1.000**	**1.000**	**0.923**	**0.908**	**0.963**	**0.942**	**0.891**	**1.000**	**1.000**	**1.000**	**0.889**	**0.945**	**0.927**
	RF	1.000	1.000	1.000	1.000	0.988	1.000	1.000	0.979	1.000	1.000	1.000	1.000	0.995	0.993
1995	**SVM**	**1.000**	**1.000**	**0.941**	**0.941**	**0.951**	**0.906**	**0.837**	**0.923**	**1.000**	**1.000**	**1.000**	**1.000**	**0.940**	**0.918**
	RF	1.000	1.000	1.000	1.000	1.000	1.000	1.000	1.000	1.000	1.000	1.000	1.000	1.000	1.000
2000	**SVM**	**1.000**	**1.000**	**1.000**	**1.000**	**0.975**	**0.940**	**0.868**	**0.943**	**1.000**	**1.000**	**1.000**	**1.000**	**0.966**	**0.955**
	RF	1.000	1.000	1.000	1.000	1.000	0.988	0.974	1.000	1.000	1.000	1.000	1.000	0.995	0.994
2004	**SVM**	**0.944**	**1.000**	**1.000**	**1.000**	**0.896**	**0.885**	**0.809**	**0.776**	**1.000**	**1.000**	**1.000**	**1.000**	**0.912**	**0.886**
	RF	0.979	1.000	1.000	1.000	0.987	1.000	1.000	0.980	1.000	1.000	1.000	0.917	0.991	0.988
2010	**SVM**	**1.000**	**1.000**	**0.889**	**0.941**	**0.952**	**0.930**	**0.911**	**0.872**	**0.727**	**1.000**	**1.000**	**1.000**	**0.937**	**0.914**
	RF	1.000	1.000	1.000	1.000	0.975	1.000	1.000	0.957	1.000	1.000	1.000	1.000	0.990	0.987
2015	**SVM**	**1.000**	**1.000**	**1.000**	**1.000**	**0.939**	**0.939**	**0.872**	**0.872**	**1.000**	**1.000**	**1.000**	**1.000**	**0.954**	**0.940**
	RF	1.000	1.000	0.969	1.000	0.988	0.988	1.000	0.974	1.000	1.000	1.000	1.000	0.991	0.988
2020	**SVM**	**1.000**	**1.000**	**1.000**	**1.000**	**0.943**	**0.957**	**0.933**	**0.913**	**1.000**	**1.000**	**1.000**	**1.000**	**0.967**	**0.957**
	RF	1.000	1.000	1.000	1.000	1.000	1.000	1.000	1.000	1.000	1.000	1.000	1.000	1.000	1.000

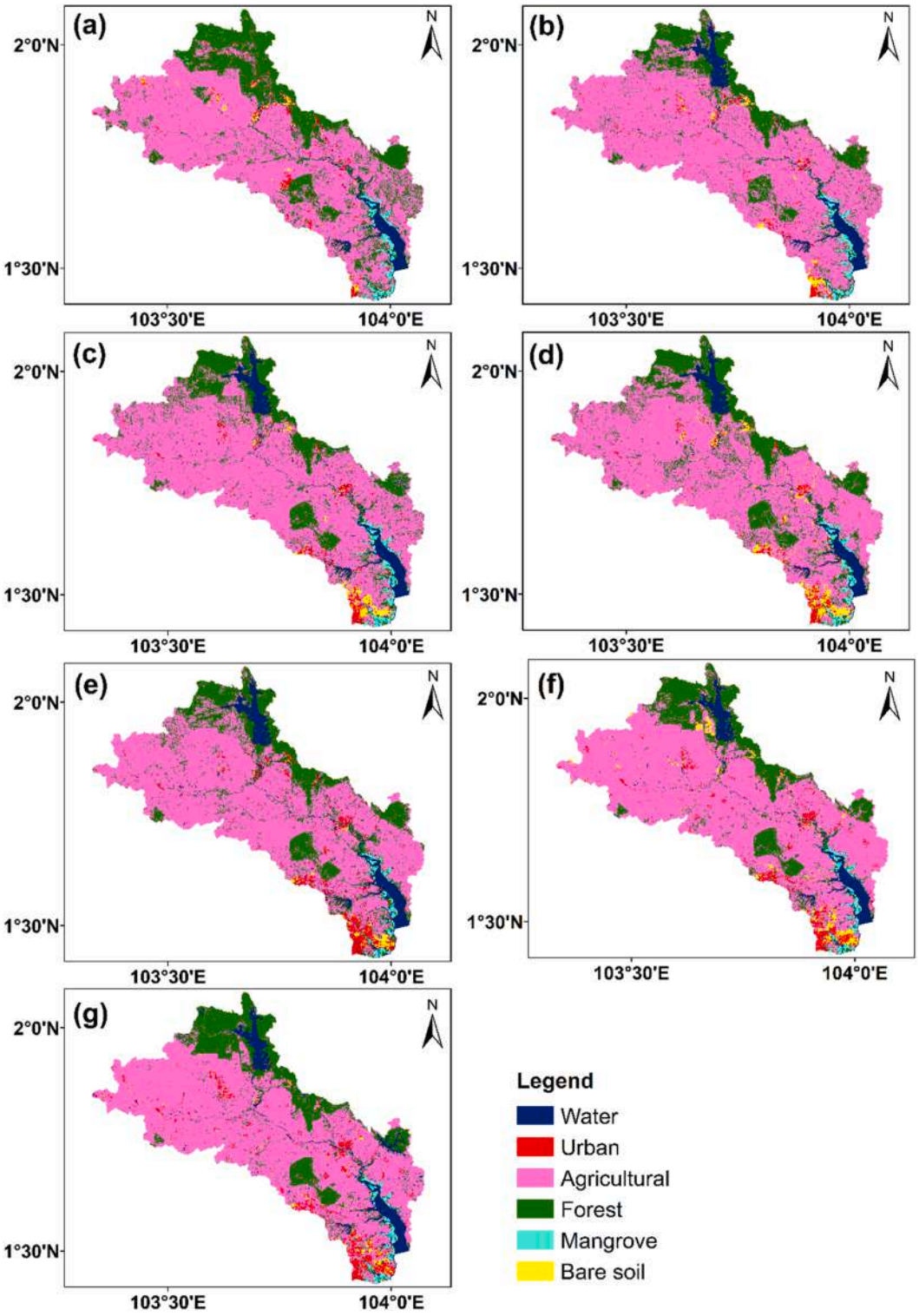

Fig. 4. Classification maps of JRB using the SVM classifier, (a) 1990, (b) 1995, (c) 2000, (d) 2005, (e) 2010, (f) 2015, and (g) 2020.

4.2. LULC change analysis

Based on the classification maps as shown in Fig. 4, the area of each class was computed as in Table 5 and plotted in Fig. 6. Over the period of the 30 years examined, a significant loss of land cover, especially forest, was identified, and the most rapid reduction of forest

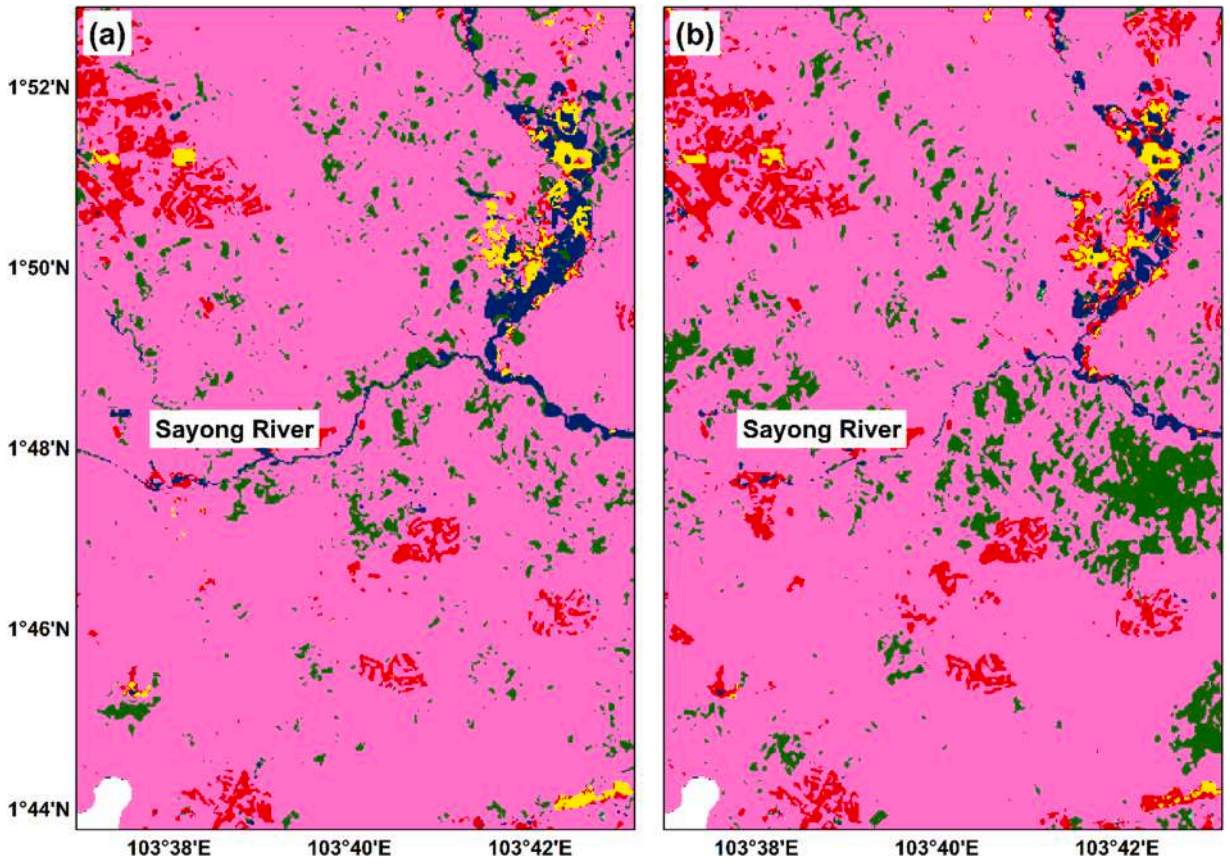

Fig. 5. Comparison of river identification based on SVM classifier (a) and RF classifier (b); classification maps of year 2020 were used to show the capability of the two classifiers to classify rivers.

was found between 1990 and 1995, with a total reduction of 20992.6 ha. In the same period, agricultural land expanded 15573.2 ha, and most of these expansions were at the expense of forest destruction. This transition of forest to agricultural land, especially oil palm, has a long history to support national income from commodity manufacturing and trading (Aznam Yusof and Bhattasali, 2008). Losses of mangrove areas were also detected during the study period. Although mangrove covers only less than 2.0% of the whole JRB region, nearly 30% of mangrove losses were identified from 1990 to 2020. Since most mangrove lands were located at the downstream of the JRB, the major loss of mangrove areas was found to be associated with the development of the Pasir Gudang Port and conversion to agricultural activities. Note that the lowest mangrove area recorded was in 2010 with 2822.2 ha, then a regrowth of mangrove was noticed in years 2015 and 2020, increasing the total mangrove land to 3081.6 ha by 2020. The regrowth of mangrove within the past 10 years can be accredited to an increasing public awareness due to the policy of the Iskandar Malaysia Regional Development Authority on mangrove conservation and restoration (Kanniah et al., 2021).

Water is an essential resource that supports the daily life of the people living in the Johor state and Singapore (Chuah et al., 2018; Heng et al., 2017). From 1990 to 1995, the construction of the Linggui dam, a reservoir with maximum capacity of 760 million cubic meters, served as the main water supply source for the area at the northern side of the JRB. The dam construction increased the coverage of water area in JRB from 8662.5 ha to 13619.9 ha, with a net increase of 4957.4 ha (57.3%). The Linggui dam project also contributed partly to the loss of forest area within this period. Another increase in water bodies is found in 2020 where the construction of another dam (Seluyut dam) increased areas covered by water to 15690.40 ha (6.6%), which is the highest of the 30 years period. Besides dams, sand mining and man-made ponding along the river for economic and agricultural usage was also found to be the reason for the widening of Johor River, which consequently increased the water area and changed the river morphology. The expansion of urban areas, i.e. the Penggerang industrial area at the southern east of the Johor coast (not in the JRB), meant that more water was demanded for industrial usage and to support the daily water needs of the population that had moved into the area. The urban expansion of the JRB rose from 4603.5 ha in 1990 to 10541.7 ha in 2020, which was more than a two-fold gain over three decades. The most rapid gain of urban area was between 2005 and 2010, which corresponds to the highest loss of bare soil area from 2005 to 2010.

A change detection analysis was conducted to show generally how each LULC class changed during the 30 years period. Based on Fig. 6 and Table 6, water, urban, and agricultural gained 6484.48 ha, 6337.53 ha, and 10699.29 ha respectively, while forest, mangrove, and bare soil lost 21919.32 ha, 1374.03 ha, and 229.95 ha, respectively. A total of 24.28% of increment of water surface was recorded while the highest gain was from the Urban class (68.55%), from 4203.81 ha rising to 10541.34 ha. Agricultural land

Table 5
Area (ha) and percentage of LULC for respective year.

	1990		1995		2000		2004		2010		2015		2020	
	Area (ha)	%	Area (ha)	%	Area (ha)	%	Area (ha)	%	Area (ha)	%	Area (ha)	%	Area (ha)	%
Water	8662.5	3.6	13619.9	5.7	13808.7	5.8	12761.2	5.3	14815.5	6.2	13690.4	5.7	15690.4	6.6
Urban	4603.5	1.9	4850.4	2.0	5458.9	2.3	5455.8	2.3	8979.4	3.8	9058.8	3.8	10541.7	4.4
Agricultural	153748.5	64.4	169321.7	71.0	162600.0	68.1	159067.0	66.7	158331.8	66.4	165028.4	69.2	161525.1	67.7
Forest	65569.1	27.5	44646.5	18.7	49488.8	20.7	52077.4	21.8	51940.1	21.8	42610.9	17.9	45298.3	19.0
Mangrove	4272.8	1.8	4017.9	1.7	4106.4	1.7	3536.3	1.5	2822.2	1.2	3062.9	1.3	3081.6	1.3
Bare soil	1758.4	0.7	2158.8	0.9	3151.4	1.3	5718.9	2.4	1724.9	0.7	5164.1	2.2	2478.2	1.0
Total	238614.8	100	238615.1	100	238614.1	100	238616.6	100	238613.9	100	238615.5	100	238615.2	100

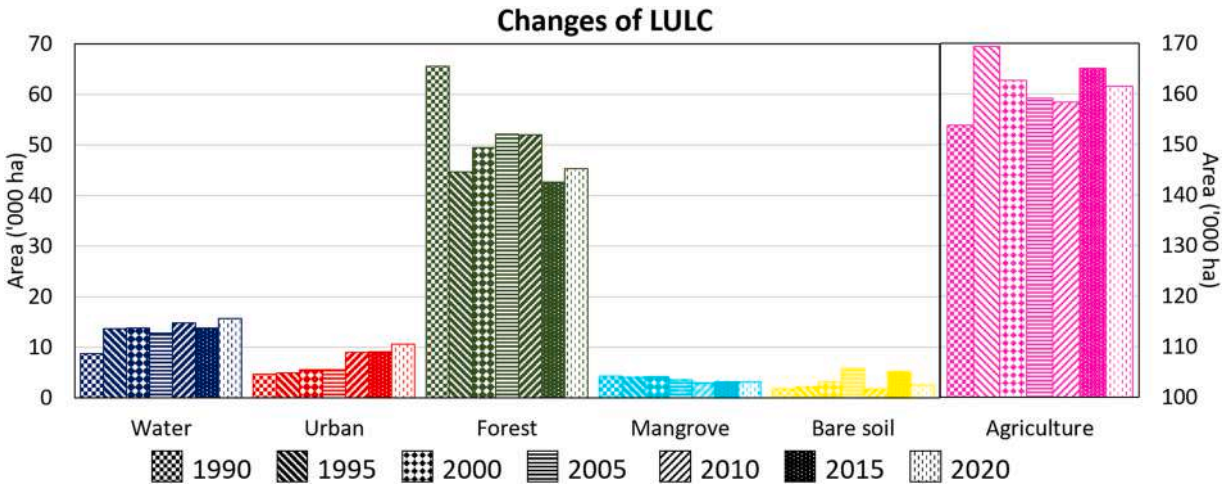

Fig. 6. Coverage area of the LULC classes of the year of investigation.

Table 6
Change detection matrix (number of pixels) between 1990 and 2020.

	Water	Urban	Agricultural	Forest	Mangrove	Bare soil	Total (2020)	Gross Gain
Water	**78893**	2119	17490	65747	7370	2714	174333	95440
Urban	2655	**14888**	70688	19691	2892	6312	117126	102238
Agriculture	10784	25843	**1491642**	246573	2810	17040	1794692	303050
Forest	5789	3402	77598	**407180**	7099	2237	503305	96125
Mangrove	3412	1	517	1808	**28500**	2	34240	5740
Bare soil	728	456	17876	5854	836	**1785**	27535	25750
Total (1990)	102261	46709	1675811	746,853	49507	30090	2651231	
Gross Loss	23368	31821	184169	339673	21007	28305		
Net Gain/Loss	72072	70417	118881	-243548	-15267	-2555		
% Changes	24.28	68.55	11.01	45.82	42.79	94.17		

gained 10692.99 ha (11.01%) over the same period. The loss of natural ecosystems (forest and mangrove) was 45.82% and 42.79%, respectively, over the 30 years period. The most significant LULC change was the transition from forest to agricultural land, where 22191.57 ha (9.3% of the total land in JRB) of forest land was cleared and used for agricultural activity. Bare soil is among the smallest LULC class but shows the highest percentage of change (94.17%), due to the rapid land clearing and urban built-up activities over the study period. A more detailed analysis of change detection at 5 years intervals can be found in the change detection matrix in the Supplementary document (Table S1 – S6).

4.3. LULC change intensity analysis

The change detection matrix at 5 years intervals (Table S1 – S6) can be used to provide information about the LULC intensity

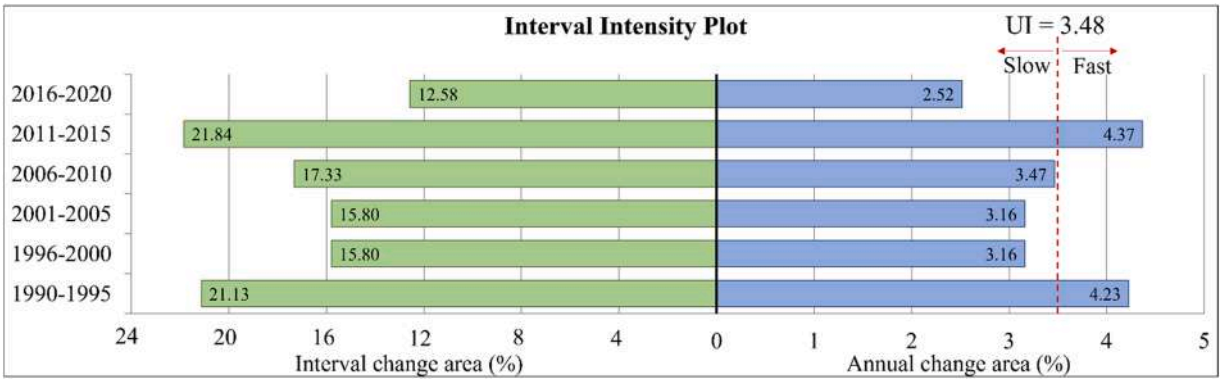

Fig. 7. Interval intensity plot for six time intervals.

analysis. Note that we used the number of pixels but not the converted area (ha) as the main unit for intensity analysis to prevent any degradation of accuracy in the analysis during the process of pixel to area conversion. Fig. 7 shows the interval intensity analysis for the JRB. The left side of the plot describes the total percentage of changed area within each interval. The highest interval change is noticed in the period between 2011 and 2015 while the period between 2016 and 2020 recorded the lowest change intensity among other periods. The right side of the plot describes how fast the area changed annually. Similarly, the fastest and slowest annual change was for periods between 2011 and 2015 and 2016 – 2020, respectively. Uniform intensity (UI), presenting the change intensity of the whole period (30 years) was calculated and compared to the annual change area rate. The uniform intensity in this study is 3.48%, where only the two intervals: 1990 – 1995 (4.23%) and 2011 – 2015 (4.37%) recorded a relatively faster rate (more intense LULC changes then normal) of change among the six periods. Three intervals (1996 – 2000, 2001 – 2005, and 2016 – 2020) were found to have a slower annual change intensity than the UI. During the interval between 2006 and 2010, the annual change rate was found to be almost similar to the UI. All the bars on the right side of the plot indicate the rate of change of the JRB was not stationary throughout the study period.

We further analysed the category intensity change for each LULC class over the 6 intervals during the 30 years period (Fig. 8). The bars on the left side of the plots indicate the annual change area (number of pixels) of each class, including their gross gain and gross loss during each interval. The bars on the right side of the plot indicate the annual change intensity of each class; if the bar is longer than the uniform intensity line, the changes of the respective class is active during the period. If the bar is shorter than the uniform

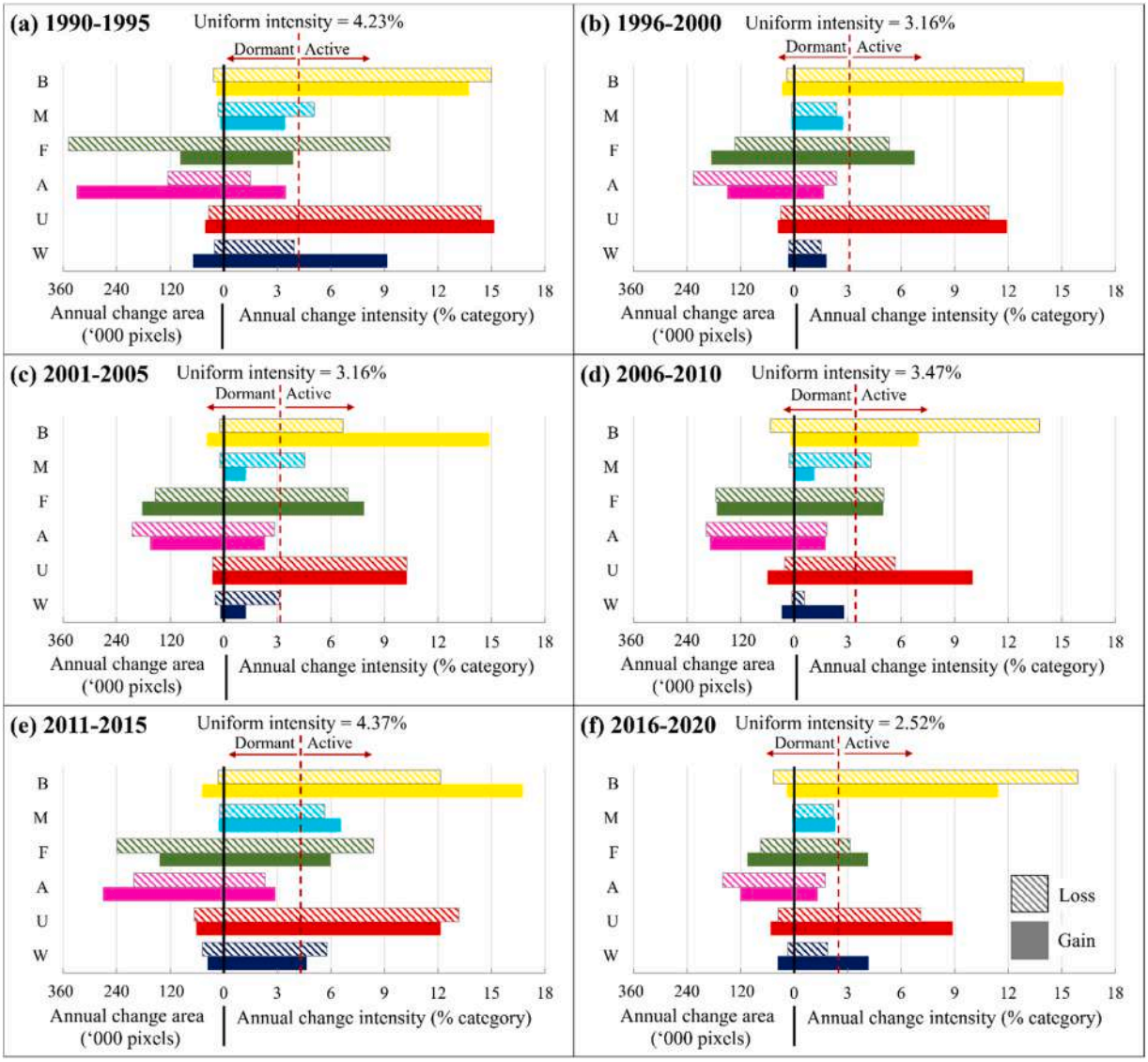

Fig. 8. Category intensity of (a) 1990–1995, (b) 1996–2000, (c) 2001–2005, (d) 2006–2010, (e) 2011–2015, and (f) 2016–2020. W = Water, U = Urban, A = Agricultural, F = Forest, M = Mangrove, and B = Bare soil.

intensity line, then the changes of the respective class is dormant during the period. It can be noticed that forest and agricultural area recorded the most gain and/or loss in each interval mainly because they have the largest coverage over the JRB and are rapidly changing. However, agricultural area and forest do not show the highest annual change intensity when compared to urban and bare soil. The bars on the right hand side of the plots indicate the annual change intensity of each class, which can explain that the LULC changes are simply due to the large size of the categoies or can be related to the intensity of changes of the category. If the bar of the gain or loss is longer than the uniform intensity (red dotted line), the change of the LULC category is relatively active. It is obvious that urban, forest, and bare soil have higher annual intensity and active changes (gain and/loss) within each interval, where depletion of forest, land clearing, and urban development are all significant factors of a rapidly developing region. The bar of gain of urban and bare soil extends over the uniform line for all the intervals, indicating the urban and bare soil gains are more intensive (active) than the other LULC.

Similarly, the bar of forest loss is always longer than the uniform line, indicating active forest loss in the JRB throughout the 30 years period. In all the plots, the annual change intensity of the agricultural land during each time interval is found to be dormant (annual changes less than the uniform intensity) despite the agricultural area annual change being the highest in most of the intervals. This indicates that although agricultural land has the highest annual gain and/or loss, the change of agricultural land was relatively consistent and dormant during the six intervals. An active gain of water was found within the 1990 – 1995, 2011 – 2015, and 2016 – 2020 periods. Over the study period, two dams were built which is the main reason for the active gain of water bodies between 1990 and 1995 (Linggui Dam) and 2016 and 2020 (Seluyut Dam). On the other hand, an active loss of water was identified between 2011 and 2015, particularly due to drought conditions resulting from an El Nino event in 2015 (Low and Loganathan, 2019).

At the transition level, we focus our analysis on the natural LULC (Forest) and the irreversible LULC (Urban) to show areas where there were forest losses, and where urban areas were gained from; and whether these transitions were systematically targeted/avoided from the specific class. Fig. 9 demonstrates the annual transition rate and intensity from forest to other LULC for each period. Higher transition intensity from forest to water was identified during the 1990 – 1995 and 2016 – 2020 intervals, particularly due to the occupancy of forest lands for dam construction. This can be explained by forest being targeted for transition to water. At the other intervals, the intensity of forest transition to agricultural, bare soil, and mangrove was higher. Targeted transition (clearance) of forest to bare soil was noticed as four out of six intervals have higher annual transition intensity of bare soil than the uniform intensity. As the urban expansion in JRB area is found doubled during the study period, we hypothesized that the clearance of forest could be targeted to urban development. However, the forest clearance does not fully contribute to the urban transition, as the annual transition intensity of urban is always below (avoided transition) the uniform intensity. This may be because part of the clearance of forest became agricultural land instead of urban land. This argument can be supported by the plots shown in Fig. 10 as: 1) the annual gain intensity of urban from forest is always below the uniform intensity of all intervals (showing systematic avoidance of transition over the period), proving that forest is not the main LULC that is targeted for urban transformation, and 2) bare soil has the highest annual transition intensity, which is always higher than the uniform intensity value of all intervals; showing that urban gains targeted bare soil more intensively compared to forest (and other categories). This condition also can be explained as bare soil is systematically targeted for transition to urban. Thus, we can conclude that direct transition from forest to urban in JRB was avoided throughout the 30 years period. Over all the intervals, the computed hypothetical annual transition errors are less than 4% in terms of accounting the apparent deviation from the uniform transitions of respective intervals. Note that the computation of hypothetical errors of uniform annual transition assumes the changes of a targeted category of the initial time allocated different area of the final time.

As shown in Fig. 8, high transition intensities from forest to bare soil, and higher transition intensities from forest to agricultural

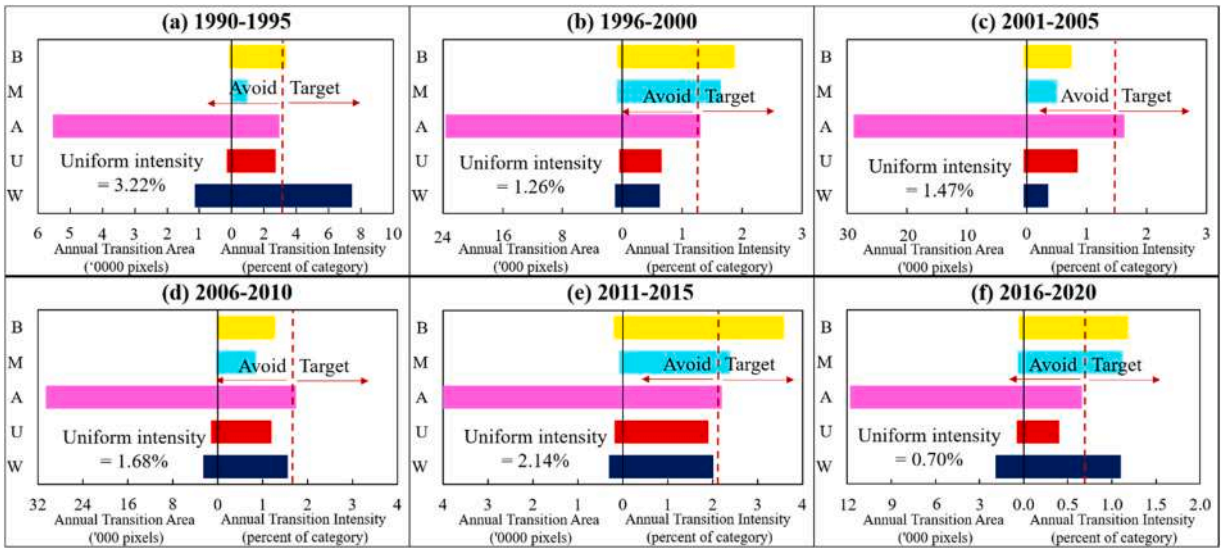

Fig. 9. Transition analysis from Forest for (a) 1990–1995, (b) 1996–2000, (c) 2001–2005, (d) 2006–2010, (e) 2011–2015, and (f) 2016–2020.

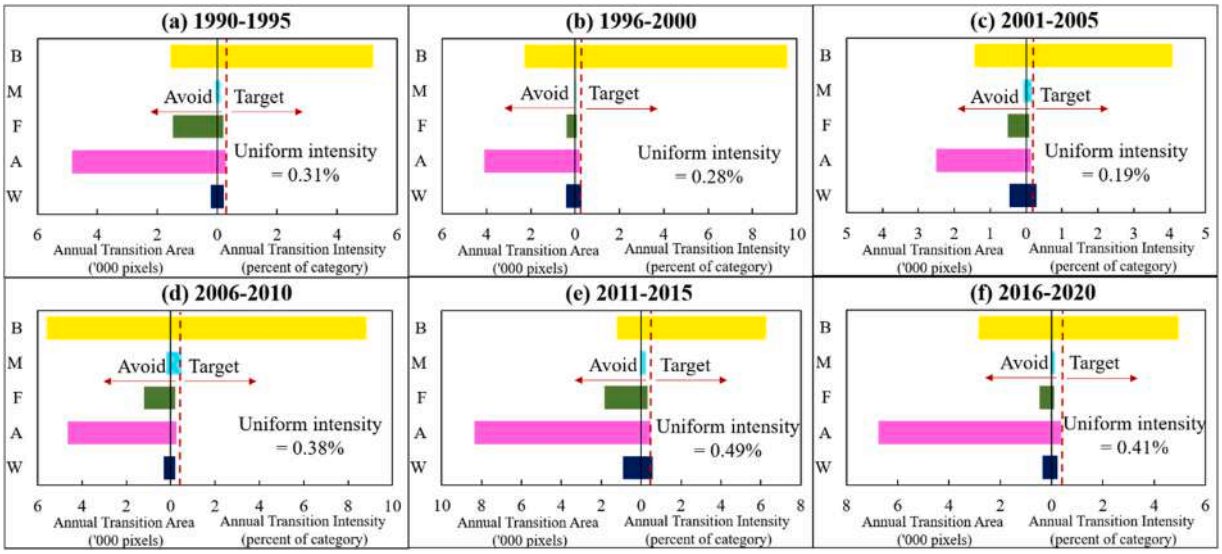

Fig. 10. Transition analysis to Urban for (a) 1990–1995, (b) 1996–2000, (c) 2001–2005, (d) 2006–2010, (e) 2011–2015, and (f) 2016–2020.

than from forest to urban (avoided transition); indicates that most of the urban conversions are from agricultural and bare soil, rather than from forest itself. Here, a detailed investigation was performed to explore the main category(ies) that contributed to the increase of urban land. Analysis of the agricultural land losses could answer this query. Fig. 11 analyzed the intensity of agricultural losses to bare soil and urban for the six intervals. Targeted clearance of agricultural land to bare soil was identified throughout the study period, where all the annual transition intensity bars are longer than the uniform line of the respective intervals. There is also targeted loss of agricultural land to urban (except 2001 – 2005). This analysis proves that the LULC changes from systematically targeting transition of agricultural to bare soil and from bare soil to urban, indicates that the LULC changes from forest to urban was avoided – direct destruction of forest land for urban uses was inactive during the study period.

4.4. River morphology analysis

Urbanization can impact the morphology of the river due to increase of streamflow, runoff, sediment transport etc. The changes that occurred on the physical properties i.e., area, length, and migration area and distance of the Johor River at every 5 years interval are presented in this section. Fig. 13 shows the overlaid river polygons to show the changes of the river boundary over the years. The centerlines and their length and areal extent derived from the Johor River are presented in Table 7. In general, the area of water increased from 5442.46 ha in 1990 to 5684.94 ha in 2020. On the other hand, the length of the centerlines increased from 1990 to 2005 then decreased from 2010 to 2020. The mean length of the centerlines is recorded as 90249.77 m. For the analysis of channel migration, the centerline of Johor River is divided into 13 reaches (Fig. 14) based on the centerline of year 1990 (as the original state).

Analysis on two outputs from the CMT are focused here including the river migration area and the river migration distance. The

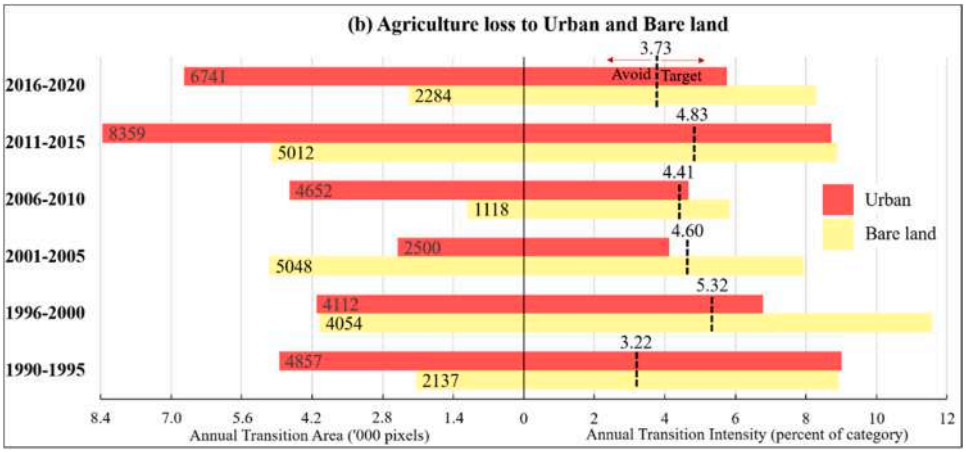

Fig. 11. Annual transition intensity plot of agricultural losses to bare soil and urban over the six intervals.

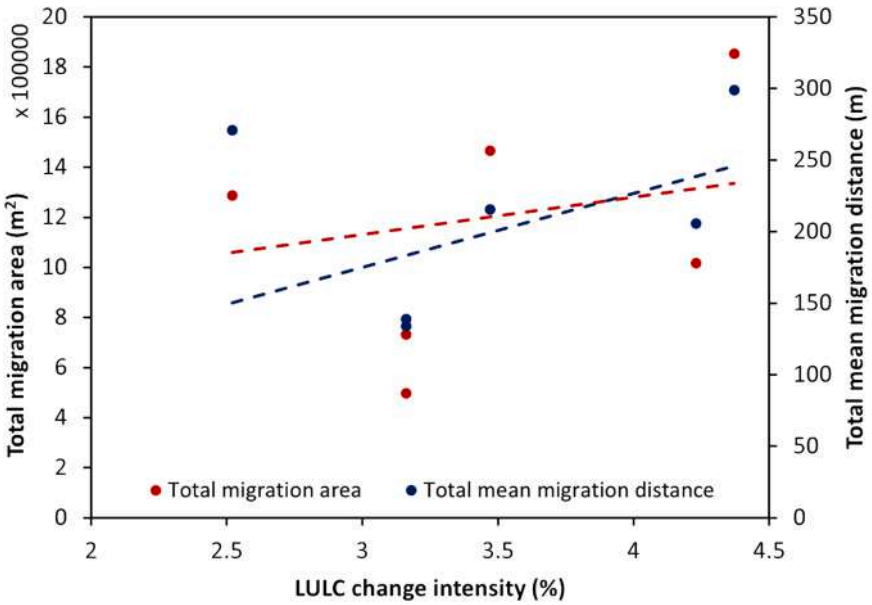

Fig. 12. Proportional relationship between LULC change intensity to total migration area and total mean migration distance.

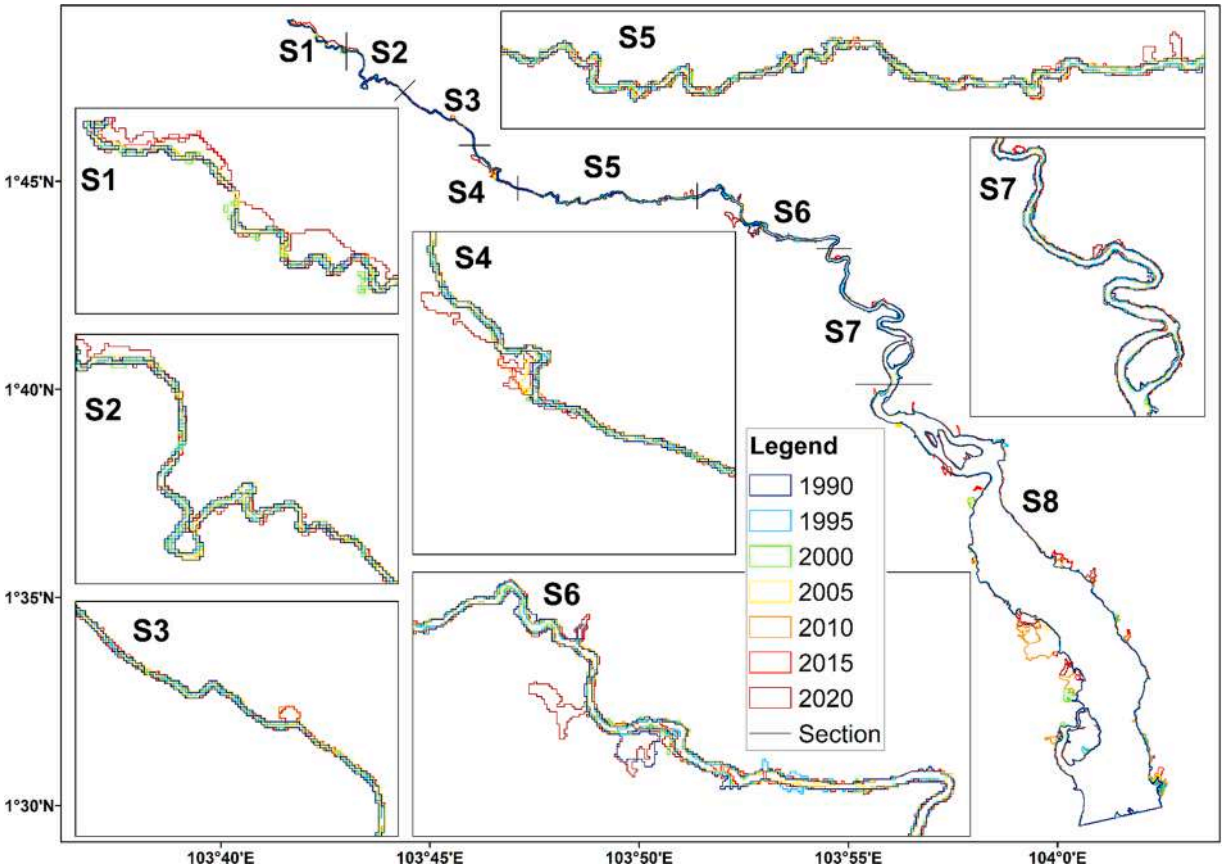

Fig. 13. Johor River boundary changes over 1990–2020, zoomed in to respective sections (S1 - S8).

Table 7
Area and the length of centerlines of Johor River focused in this study.

Year	Area	Length
1990	5488.62	89928.77
1995	5384.74	90964.90
2000	5396.37	91261.31
2005	5372.03	91294.96
2010	5711.05	90451.75
2015	5547.66	89518.95
2020	5683.61	88327.78

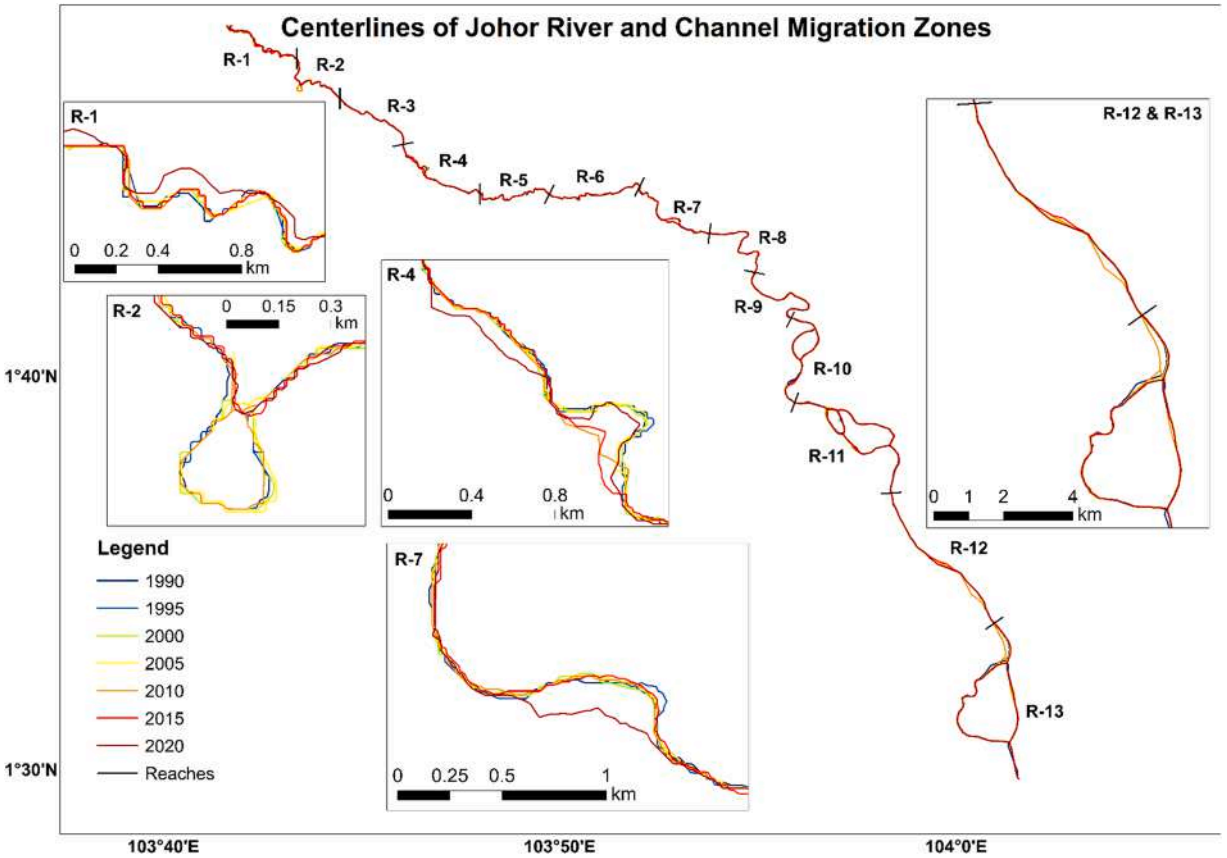

Fig. 14. Centerlines of river and channel migration zones over 30 years within the Johor River Basin.

river migration area refers to the area of polygons generated by overlaying the centerlines of subsequent years. The river migration distance refers to the distance detected by overlaying the transects at specific locations along the centerlines. Table 8 explains the trends of Johor River migration over the study period. Table 8 (a) shows the migration zones within each reach, their total migration, and the total polygons generated along the river over each interval; and Table 8 (b) reported the migrated distance detected by all the transects within each reach (mean migration distance) and their total over each period. Less migrated (changed) portion of the river is found within R-5 to R-9 (*italicized*) (Table 8 (a & b)). In general, highest area migration (1853886 m^2) of Johor River occurred between 2010 and 2015 and least area migration (498609 m^2) occurred from 1995 to 2000. We compared the annual change intensity (Fig. 7) with the total migration area and total migration distance as shown in Fig. 12. The proportional relationship between LULC changes intensity with the total migration area and total mean migration distance shows that higher LULC change intensity can lead to higher river migration, which could increase the river morphology changes over the respective period. Therefore, the result implies that LULC changes can impact the river morphology of the JRB.

Among the reaches, higher migration (shaded in Table 8 (a)) occurred in R-12 (1188252 m^2) and R-13 (1986384 m^2). This situation could be due to the R-12 and R-13 are located near the estuary, which has the widest width along the Johor River, where a slight changes on the centerline will cause higher migration of area over these reaches. Fig. 15 (a) showed the maps of the locations of R-12 and R-13. From Fig. 13, significant changes at both sides of R-12 and R-13 can be seen, where on the left side of the river, some areas

Table 8
Channel migration area (a) and mean channel migration distance (b) of Johor River.

(a)	Migration Area (m^2)													**Total**	**No. of polygons**
	R-1	R-2	R-3	R-4	R-5	R-6	R-7	R-8	R-9	R-10	R-11	R-12	R-13		
1995	42953.0	42739.2	27461.0	38559.3	*41442.1*	*45726.2*	*42956.9*	*36742.3*	*42553.3*	112537.7	88916.3	77733.5	377207.2	1017528	570
2000	31248.7	18989.1	21061.3	30286.5	*31006.9*	*20599.0*	*38734.5*	*21523.5*	*23008.5*	48742.5	32665.3	69125.1	111617.8	498609	501
2005	60117.5	44103.3	49065.7	43167.6	*45974.0*	*48029.5*	*50176.2*	*29957.0*	*34315.8*	53195.0	89019.4	69230.1	116250.0	732601	603
2010	46086.0	49651.4	43643.0	88633.7	*38652.6*	*37321.6*	*42218.9*	*29913.3*	*29029.3*	62590.6	86379.2	349704.8	562878.5	1466703	659
2015	68220.5	87062.9	41337.9	59406.6	*43572.5*	*45785.7*	*60174.8*	*53836.5*	*48818.9*	75757.8	169984.1	412795.8	687132.3	1853886	448
2020	145134.8	42224.5	44451.4	130976.8	*48892.2*	*45378.9*	*156334.8*	*47909.4*	*43709.9*	89785.9	152751.2	209662.5	131298.0	1288510	439
	393760.5	284770.4	227020.3	391030.4	*249540.4*	*242840.8*	*390596.1*	*219882.0*	*221435.7*	442609.5	619715.4	**1188251.7**	**1986383.8**		
(b)	**Mean Migration Distance (m)**													**Total**	
	R-1	**R-2**	**R-3**	**R-4**	**R-5**	**R-6**	**R-7**	**R-8**	**R-9**	**R-10**	**R-11**	**R-12**	**R-13**		
1995	14.66	35.12	11.17	14.70	*21.65*	*7.90*	*2.19*	*8.30*	*19.70*	10.54	11.72	6.79	41.27	205.72	
2000	14.21	7.92	14.99	17.32	*12.86*	*9.97*	*9.55*	*6.31*	*12.78*	11.51	4.47	3.12	9.03	134.03	
2005	13.52	15.18	13.86	9.00	*11.87*	*13.09*	*10.50*	*4.52*	*6.52*	12.14	8.80	8.50	11.34	138.84	
2010	12.10	21.00	9.96	33.98 *	*6.85*	*7.43*	*9.58*	*6.00*	*2.80*	6.53	46.22	8.60	44.58	215.62	
2015	17.28	45.25 *	12.51	7.80	*9.16*	*14.50*	*17.20*	*12.38*	*12.33*	9.26	26.66	56.89	57.93	299.15	
2020	41.30 *	10.33	15.47	38.30 *	*6.83*	*15.22*	*40.92 **	*14.39*	*4.33*	8.35	28.75	34.01	12.68	270.86	
	113.06	134.80	77.96	121.09	*69.22*	*68.10*	*89.94*	*51.89*	*58.46*	58.33	126.62	117.92	176.84		

*Values selected for detail analysis on migration distance.

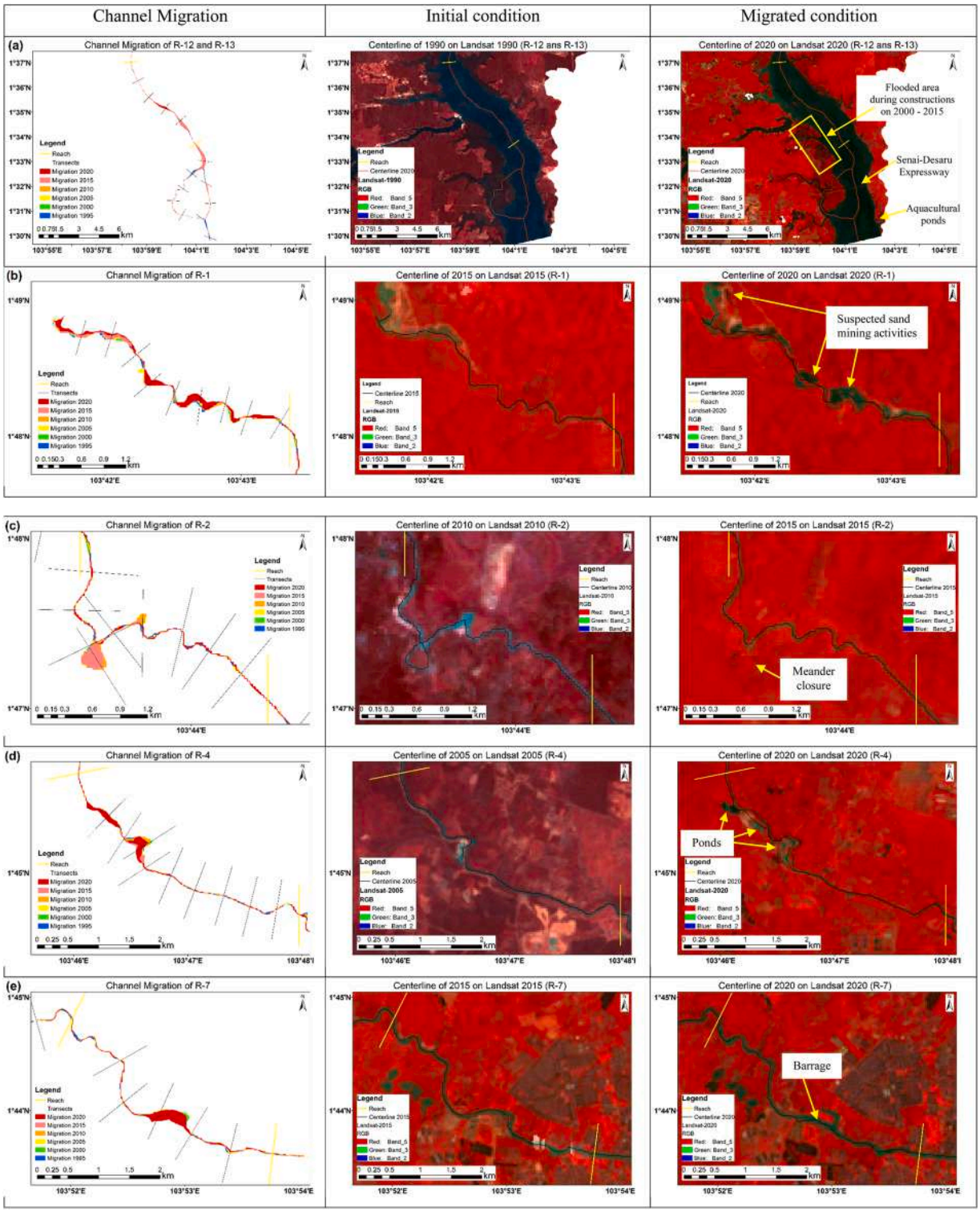

Fig. 15. Specific locations of river morphology changes in Johor River by reach(es); (a) R-12 and R-13 near the estuary of the river, (b) R-1 at the outlet of Linggui dam, (c) R-2 showing a meander closure, (d) R-4 indicates riverside ponding for agricultural usage, and (e) R-7 near Kota Tinggi town where a barrage was built.

were covered by water in 2010 but no water remained after 2015. We suspect this could be due to heavy development of the area, where the Senai-Desaru Expressway (indicated in Fig. 15 (a)) was built, which caused serious mangrove degradation and led to flooding in 2010. Moreover, on the right side of R-13, development of aquacultural activities were noticed, which could be the main reason that contributed to the high changes recorded. Land reclamation (Wang et al., 2019) near the estuary of Johor River could also contributes to the high channel migration.

Table 8 (b) captures more details of channel migration at specific locations. Several high mean migration distance values were detected and analyzed (values with asterisk). R-1 recorded relatively higher migration distance throughout the study period. The main reason for the high migration distance is because this area is located at the outlet of Linggui dam built on year 1992, where most of the impacts following the construction of dams could be detected. Highest migration distance of R-1 was detected over year 2015–2020, where a mean of 41.30 m of migration was recorded from the 10 transects generated within this reach. Fig. 15 (b) highlighted the changes of R-1. Several sand mining activities were noticed along the main river and these activities created ponding of water besides the river, which have been classified as part of the river based on our classification algorithm. The ponds created by sand mining activities can be clearly identified from the LULC classification map of year 2020, where forest and agricultural land were cleared for the purpose of sand mining. The presence of these sand mining ponds (changes occurred in LULC) increased the migration area and distance of the river (river morphology of R1) as shown in Table 8. Sand mining near the river, if not properly managed, can bring a negative impact to the river itself and the surrounding environment and ecosystem, including shallowing the river and increasing sediment flow downstream.

Fig. 15 (c) displayed a meander closure along the R-2 between year 2010 and 2015, resulting a mean migration distance of 45.25 m. The inlet of the river meander was found to be filled with soil, possible reasons for this are due to the shortening of river or to avoid flooding over the plantation zone. Another high mean migration distance was detected due to plantation activities within R-4 between year 2005–2020 (Fig. 15 (d)). Total mean migration distance of this reach from 2005 to 2020 is recorded as 80.08 m. Over this area, ponds built along the river have been classified as the river. Since about 65% of the JRB is agricultural land, these ponds were built to store water for irrigation purposes. Water from the river can flow into these ponds and support the surrounding plantation activities. These ponds are located closely to the main river and have been classified as Water in the LULC maps, which we think could bring great impact to the river morphology changes. Therefore, we include the area of ponds classified as the river in the analysis to show the impacts of these man-made ponds to the morphology changes. In addition, a barrage was built at the Kota Tinggi town (R-7) in 2017 to prevent the saline water flow to the upper stream (Lee & binti Zaharuddin, 2015) and to prevent floods (Fig. 15 (e)). Channel migration distance of 40.92 m was reported due to the change of water course and the barrage separated the river into two parts and increased the water area surrounding it. The existence of the barrage could influence the biodiversity of the area, impacting the fishery production due to a reduced flow of saline water (Sinha et al., 1996).

Through the analysis of migration area and migration distance computed based on the river centerlines using the CMT, the shape and width changes of Johor River is analysed. Changes of the shape and width of Johor River will affect the creation of the centerlines, while the migration of centerlines can represent the changes of the river morphology during a specified area and period. This section proved that significant morphology changes on Johor River was identified, where the largest changes found near the estuary of the river. Several locations with high migration distances were identified and proved that some human-induced activities are the main causes of river morphology changes.

5. Discussion

5.1. LULC monitoring using GEE

Remote sensing and geospatial technologies offer unique opportunities in mapping, monitoring and quantitative analysis of land surface processes, such as land degradation and deforestation and their impact on the biosphere (Dubovyk, 2017). Remote sensing has been used to classify LULC since the launch of Landsat satellites in 1970 s (Souza-Filho et al., 2016). Although Landsat data are available at every 16-day intervals, frequent cloud cover, especially in the tropical/maritime regions like Malaysia, make only very few images available for producing change detection maps. Nevertheless, compositing procedures (mosaicking clear pixels) from available partially cloudy images have been developed (Roy et al., 2010). The Google Earth Engine (GEE) has become a popular platform for remote sensing image processing to eliminate clouds and LULC monitoring. Despite the GEE provides comprehensive image composite method; some issues are still noticeable on the composite images. One of the issues is the presence of cloud shadow which could not be detected and removed based on the C Function of Mask (CFMask) algorithm used by Landsat on GEE. To overcome this issue, an improved cloud shadow filter must be developed in the near future (Barboza Castillo et al., 2020), specifically over the tropical region. LULC classification in this study using GEE with SVM and RF classifiers showed high classification accuracy (OA $>$ 0.90) and SVM classifier was found advantageous on classifying narrow features as suggested by Heydari and Mountrakis (2018); Zagajewski et al. (2021). The capability of SVM to classify narrow river could be due to the non-linear hyperplanes theory which can successfully delineate water pixels surrounding by other LULC classes; while RF which is based on the ensemble tree theory could mis-group the water pixels into the other LULC classes during the voting process. Generally, the use of GEE increases the classification speed from the perspective of satellite data collection, processing, classification, and accuracy assessment. The methodology of this study can be utilized to a larger region (i.e. state and national scale) to enhance the LULC classification in terms of time and cost consumptions. Future study can utilize high spatial resolution remote sensing data which can improve the accuracy of LULC classification and change detection, and includes the digital elevation model (DEM) as input of slope during river centerline generation in order to enhance the quality of river morphology changes identification.

5.2. LULC Changes and Impacts

Increased food production due to population growth has caused large scale forest clearance in the SEA as a whole over the last 50 years (Maja and Ayano, 2021). Similarly, rapid growth in industrialization, urbanization and aquaculture have also contributed to loss of arable lands and coastal ecosystems (Sejati et al., 2020). Extensive urbanization increases water scarcity issues which leads to the construction of dams and exploration of groundwater (Chen and Trias, 2020). Impacts of LULC changes of river basins has been extensively studied and linked to climate change (temperature, precipitation etc.) and alteration of hydrological processes (runoff, discharge, floods, streamflow, evapotranspiration, lateral flow etc.) (Chanapathi and Thatikonda, 2020; Getachew et al., 2021; Petchprayoon et al., 2010; Sinha et al., 2020; Zope et al., 2017). Deforestation and urbanization are two key factors that contribute to LULC changes of a river basin, while the building of a reservoir or dam within a river basin has become very common in recent years (Behera et al., 2018; Li et al., 2020; Woldemichael et al., 2012) to overcome water related issues. The Johor River Basin is an area where tropical flora and fauna presents, but population growth and urbanization have altered the LULC of the area dramatically as shown in this study. The findings of this study are similar to our previous LULC study of the Iskandar Malaysia Development Region (Kanniah et al., 2015), where loss of natural land cover (forest and mangrove) and gain of agricultural, urban, and bare soil were identified. A total of 8.5% of forest loss and 0.5% of mangrove loss were identified during the study period in JRB, which were converted into dams, agricultural lands, urban area, and cleared bare soil. To ensure water security for the local population and support regional (Singapore) necessity, dams were built in the JRB. Construction of a dam can have a strong impact on the river ecosystem where river flow regulations, river channelization, water abstraction are among the most influencing factors that cause river stress (Sabater et al., 2018). The building of dams increased the areas covered by water in the study area, where an increase of 4957.4 ha and 2000 ha were identified between 1990 and 1995 and 2015 – 2020, corresponding to the period when the Linggui and the Seluyut dams were built, respectively. Besides damming, building of a barrage, and human exploration (sand mining) were also identified along the river. Changes of the rivers in a basin can have socio-economic, biodiversity, hydrology, and environmental impacts. Consequently, the changes of these LULC could have caused changes in the river morphology. From this study, we identified the increase of water area when analyzing the main river (Johor River) in the JRB, which was mainly due to damming, building of a barrage, and human exploration (sand mining).

Inconsistencies in LULC change based on the intensity analysis in this study (Fig. 7 to Fig. 11) clearly show the intensity of the LULC changes, particularly the depletion of forests and agricultural lands for water (dams) and urban development. Within each interval, at least 12% of land area was changed within JRB. Approximately 25% of area changes was identified on two intervals (1990 – 1995 and 2010 – 2015). The high area changes occurred between 1990 and 1995 could be due to the introduction of New Development policy of the Malaysia government while the development of Iskandar Malaysia region could be the reason for high changes occurred between year 2010–2015. The detailed analysis highlights hotspots in LULC change of bare soil (94.17%), urban (68.55%), forest (45.82%), and mangrove (42.79%) and it is useful to local stakeholders and policy makers for regulating and realizing sustainable development goals (SDGs) to prevent over exploration of land and resources in the area. The expansion of oil palm and rubber plantation lands in the JRB over the past decades is found to correspond to the regional pattern. Gains and losses of bare soil were found always active over the study period, indicating active forest clearance to bare soil and active transition of bare soil to urban development, which is particular pattern of a rapidly developing region. As it has been suggested previously, this intensify LULC changes could bring severe impacts to the area, including the changes of river morphology.

5.3. River morphology changes

Based on the Channel Migration Toolbox, the area and distance changes of the Johor River was detected based on the polygons and centerlines generated from the classification results. Higher river migration (area and mean distance) was identified during the period when there is higher LULC change intensity and vice versa (Fig. 12). This finding supports our hypothesis that LULC changes can impact the river morphology in JRB. Changes of river morphology usually can only be detected over decades but human interference can directly induced channel adjustments (Surian and Rinaldi, 2003). Recent studies concentrated on examining river morphology changes following the construction of dams (Li et al., 2020; Piqué et al., 2016) and flood events (Magliulo and Valente, 2020; Yousefi et al., 2019), and found that these activities contribute to river morphology changes at different magnitudes due to the characteristics of the study area. Dingle et al. (2019) concludes that tropical river characterized with higher channel migration rate then temperate. However, research on river morphological changes is found limited in the Southeast Asia. From the analysis, most of the migration captured in this study are human-induced, including mangrove degradation due to expressway construction (R-12 and R-13), dam construction and sand mining activities (R-1), agricultural activities (R-2 and R-4), and the construction of barrage (R-7). These anthropogenic activities, although mainly targeted to improve humans' livelihood, particularly over the high populated area, should be planned with a boarder perspective and according to international and local policies to prevent habitat fragmentation, ecological impacts, and assure water security and environmental sustainability (Hohensinner et al., 2018; Spada et al., 2018). Further research is required to explain the changes of the area of river over the time, since these changes are mainly due to the combined effects of natural (rainfall, runoff, drought, tides, etc.) and manmade activities (sand mining, aquaculture conversion, etc.). The method introduced in this study can be developed as a toolkit to consistently investigate the migration and morphological changes of the rivers in the region.

6. Conclusion

This study investigated the LULC changes of the Johor River Basin and the changes of river morphology over the period 1990–2020,

based on remote sensing and GIS techniques. The Google Earth Engine was applied with Landsat imageries and two classifiers (SVM and RF) were compared. High classification accuracy was achieved with an overall accuracy above 90%, while SVM produced more detailed classification maps compared to RF with better capability to detect narrow river features. Increase of Water and Urban area based on the classification results indicate that JRB is a hotspot of urbanization with increasing water demand with the construction of two dams. The main river (Johor River) in the JRB was selected for river morphology change analysis. Intensity analysis on the classification results shows an average of 3.48% of JRB area underwent LULC changes annually. Forest, Urban, and Bare soil are the classes changing actively throughout the 30 years period. Activities including sand mining, artificial meander closure, and barrage construction were identified along the Johor River, and the impacts of these activities to the river migration is highlighted in this study. However, the impacts of these anthropogenic modifications to the ecosystem and environment are unknown. A better understanding on how the LULC and river morphology changes in this river basin impacts the environment, hydrological processes, ecosystem services, social and communities will become a critical subject to enhance and sustain future planning and management, to ensure water security and protect a sustainable livelihood of the area.

Declaration of Competing Interest

The authors declare that they have no known competing financial interests or personal relationships that could have appeared to influence the work reported in this paper.

Acknowledgments

We acknowledge the Universiti Teknologi Malaysia, Malaysia (through research grant Q.J130000.2452.08G51, Q.J130000.3052.02M01, and Q.J130000.3052.02M11) for providing funding to conduct the study. We thank the reviewers for their constructive comments and suggestions to improve this work.

Appendix A. Supporting information

Supplementary data associated with this article can be found in the online version at doi:10.1016/j.ejrh.2022.101072.

References

Aldwaik, S.Z., Pontius, R.G., 2012. Intensity analysis to unify measurements of size and stationarity of land changes by interval, category, and transition. Landsc. Urban Plan. 106 (1), 103–114. https://doi.org/10.1016/j.landurbplan.2012.02.010.

Amani, M., Ghorbanian, A., Ahmadi, S.A., Kakooei, M., Moghimi, A., Mirmazloumi, S.M., Moghaddam, S.H.A., Mahdavi, S., Ghahremanloo, M., Parsian, S., Wu, Q., Brisco, B., 2020. Google earth engine cloud computing platform for remote sensing big data applications: a comprehensive review. IEEE J. Sel. Top. Appl. Earth Obs. Remote Sens. 13, 5326–5350. https://doi.org/10.1109/JSTARS.2020.3021052.

Awang Ali, A.N., Ariffin, J., Mohd. Razi, M.A., Jazuri, A., 2017. Environmental degradation: a review on the potential impact of river morphology. MATEC Web Conf. 103, 04001. https://doi.org/10.1051/matecconf/201710304001.

Aznam Yusof, Z., & Bhattasali, D. (2008). Economic Growth and Development in Malaysia.

Barboza Castillo, E., Turpo Cayo, E.Y., de Almeida, C.M., Salas López, R., Rojas Briceño, N.B., Silva López, J.O., Barrena Gurbillón, M.Á., Oliva, M., Espinoza-Villar, R., 2020. Monitoring WILDFires in the Northeastern Peruvian Amazon USING landsat-8 and sentinel-2 imagery in the GEE platform. ISPRS Int. J. Geo-Inf. 9 (10), 564. ⟨https://www.mdpi.com/2220-9964/9/10/564⟩.

Behera, M.D., Tripathi, P., Das, P., Srivastava, S.K., Roy, P.S., Joshi, C., Behera, P.R., Deka, J., Kumar, P., Khan, M.L., Tripathi, O.P., Dash, T., Krishnamurthy, Y.V.N., 2018. Remote sensing based deforestation analysis in Mahanadi and Brahmaputra river basin in India since 1985. J. Environ. Manag. 206, 1192–1203. https://doi.org/10.1016/j.jenvman.2017.10.015.

Belgiu, M., Drăguţ, L., 2016. Random forest in remote sensing: a review of applications and future directions. ISPRS J. Photogramm. Remote Sens. 114, 24–31. https://doi.org/10.1016/j.isprsjprs.2016.01.011.

Breiman, L., 2001. Random forests. Mach. Learn. 45 (1), 5–32. https://doi.org/10.1023/A:1010933404324.

Brovelli, M.A., Sun, Y., Yordanov, V., 2020. Monitoring forest change in the Amazon using multi-temporal remote sensing data and machine learning classification on google earth engine. ISPRS Int. J. Geo-Inf. 9 (10), 580. ⟨https://www.mdpi.com/2220-9964/9/10/580⟩.

Chanapathi, T., Thatikonda, S., 2020. Investigating the impact of climate and land-use land cover changes on hydrological predictions over the Krishna river basin under present and future scenarios. Sci. Total Environ. 721, 137736 https://doi.org/10.1016/j.scitotenv.2020.137736.

Chen, C., Trias, A.P. L. (2020). Water Security in Southeast Asia: Regional, National, and Sub-national Challenges.

Chin, A., 2006. Urban transformation of river landscapes in a global context. Geomorphology 79 (3), 460–487. https://doi.org/10.1016/j.geomorph.2006.06.033.

Chuah, C.J., Ho, B.H., Chow, W.T.L., 2018. Trans-boundary variations of urban drought vulnerability and its impact on water resource management in Singapore and Johor, Malaysia. Environ. Res. Lett. 13 (7), 074011 https://doi.org/10.1088/1748-9326/aacad8.

Congalton, R.G., Green, K., 2019. Assessing the Accuracy of Remotely Sensed Data: Principles and Practices. CRC Press.

Dabija, A., Kluczek, M., Zagajewski, B., Raczko, E., Kycko, M., Al-Sulttani, A.H., Tardà, A., Pineda, L., Corbera, J., 2021. Comparison of support vector machines and random forests for Corine land cover mapping. Remote Sens. 13 (4), 777. ⟨https://www.mdpi.com/2072-4292/13/4/777⟩.

Deilmai, B.R., Ahmad, B.B., Zabihi, H., 2014. Comparison of two Classification methods (MLC and SVM) to extract land use and land cover in Johor Malaysia. IOP Conf. Ser.: Earth Environ. Sci. 20, 012052 https://doi.org/10.1088/1755-1315/20/1/012052.

Dingle, E.H., Paringit, E.C., Tolentino, P.L.M., Williams, R.D., Hoey, T.B., Barrett, B., Long, H., Smiley, C., Stott, E., 2019. Decadal-scale morphological adjustment of a lowland tropical river. Geomorphology 333, 30–42. https://doi.org/10.1016/j.geomorph.2019.01.022.

Dorofki, M., Elshafie, A.H., Jaafar, O., Karim, O.A., Mastura, S., 2012. Comparison of artificial neural network transfer functions abilities to simulate extreme runoff data. Int. Proc. Chem. Biol. Environ. Eng. 33, 39–44.

Dubovyk, O., 2017. The role of remote sensing in land degradation assessments: opportunities and challenges. Eur. J. Remote Sens. 50 (1), 601–613. https://doi.org/10.1080/22797254.2017.1378926.

Ekumah, B., Armah, F.A., Afrifa, E.K.A., Aheto, D.W., Odoi, J.O., Afitiri, A.-R., 2020. Assessing land use and land cover change in coastal urban wetlands of international importance in Ghana using Intensity Analysis. Wetl. Ecol. Manag. 28 (2), 271–284. https://doi.org/10.1007/s11273-020-09712-5.
Enaruvbe, G.O., Pontius, R.G., 2015. Influence of classification errors on intensity analysis of land changes in southern Nigeria. Int. J. Remote Sens. 36 (1), 244–261. https://doi.org/10.1080/01431161.2014.994721.
Estoque, R.C., Murayama, Y., 2015. Intensity and spatial pattern of urban land changes in the megacities of Southeast Asia. Land Use Policy 48, 213–222. https://doi.org/10.1016/j.landusepol.2015.05.017.
Fang, Y., Ceola, S., Paik, K., McGrath, G., Rao, P.S.C., Montanari, A., Jawitz, J.W., 2018. Globally universal fractal pattern of human settlements in river networks. Earth's Future 6 (8), 1134–1145. https://doi.org/10.1029/2017EF000746.
Feizizadeh, B., Omarzadeh, D., Kazemi Garajeh, M., Lakes, T., Blaschke, T., 2021. Machine learning data-driven approaches for land use/cover mapping and trend analysis using Google Earth Engine. J. Environ. Plan. Manag. 1–33. https://doi.org/10.1080/09640568.2021.2001317.
Fernandes, M.R., Aguiar, F.C., Martins, M.J., Rivaes, R., Ferreira, M.T., 2020. Long-term human-generated alterations of Tagus River: effects of hydrological regulation and land-use changes in distinct river zones. Catena 188, 104466. https://doi.org/10.1016/j.catena.2020.104466.
Gandharum, L., Hartono, D.M., Karsidi, A., Ahmad, M., 2022. Monitoring Urban Expansion and Loss of Agriculture on the North Coast of West Java Province, Indonesia, Using Google Earth Engine and Intensity Analysis. Sci. World J. 2022, 3123788 https://doi.org/10.1155/2022/3123788.
Geng, X., Wang, X., Yan, H., Zhang, Q., Jin, G., 2015. Land use/land cover change induced impacts on water supply service in the upper reach of Heihe River Basin. Sustainability 7 (1), 366–383. ⟨https://www.mdpi.com/2071-1050/7/1/366⟩.
Getachew, B., Manjunatha, B.R., Bhat, H.G., 2021. Modeling projected impacts of climate and land use/land cover changes on hydrological responses in the Lake Tana Basin, upper Blue Nile River Basin, Ethiopia. J. Hydrol. 595, 125974 https://doi.org/10.1016/j.jhydrol.2021.125974.
Gorelick, N., Hancher, M., Dixon, M., Ilyushchenko, S., Thau, D., Moore, R., 2017. Google earth engine: planetary-scale geospatial analysis for everyone. Remote Sens. Environ. 202, 18–27. https://doi.org/10.1016/j.rse.2017.06.031.
Guppy, L., Anderson, K. (2017). Water crisis report. *United Nations University Institute for Water*.
Harden, C.P., 2006. Human impacts on headwater fluvial systems in the northern and central Andes. Geomorphology 79 (3), 249–263. https://doi.org/10.1016/j.geomorph.2006.06.021.
Heng, H., Pan, W., Siaw, F., Hii, C., 2017. Coastal and estuary reservoir: case studies for Johor river basin. J. Civil Eng. Sci. Technol. 8 (1), 25–40.
Heydari, S.S., Mountrakis, G., 2018. Effect of classifier selection, reference sample size, reference class distribution and scene heterogeneity in per-pixel classification accuracy using 26 Landsat sites. Remote Sens. Environ. 204, 648–658.
Himayoun, D., Roshni, T., 2020. Geomorphic changes in the Jhelum River due to an extreme flood event: a case study. Arab. J. Geosci. 13 (1), 23. https://doi.org/10.1007/s12517-019-4896-9.
Hohensinner, S., Hauer, C., Muhar, S., 2018. River morphology, channelization, and habitat restoration. In: Schmutz, S., Sendzimir, J. (Eds.), Riverine Ecosystem Management: Science for Governing Towards a Sustainable Future. Springer International Publishing, pp. 41–65. https://doi.org/10.1007/978-3-319-73250-3_3.
Ibitoye, M.O., 2021. A remote sensing-based evaluation of channel morphological characteristics of part of lower river Niger, Nigeria. SN Appl. Sci. 3 (3), 340. https://doi.org/10.1007/s42452-021-04215-1.
Ismail, A.Z., Yusop, Z., Yusof, Z., 2015. Comparison of flood distribution models for Johor River basin. J. Teknol. 74 (11).
Ju, Z., Tan, M.L., Samat, N., & Chang, C.K. (2021). Comparison of Landsat 8, Sentinel-2 and spectral indices combinations for Google Earth Engine-based land use mapping in the Johor River Basin, Malaysia.
Kanniah, K.D., 2017. Quantifying green cover change for sustainable urban planning: a case of Kuala Lumpur, Malaysia. Urban For. Urban Green. 27, 287–304. ://WOS:000418470600033.
Kanniah, K.D., Kang, C.S., Sharma, S., Amir, A.A., 2021. Remote sensing to study mangrove fragmentation and its impacts on leaf area index and gross primary productivity in the South of Peninsular Malaysia. Remote Sens. 13 (8), 1427. ⟨https://www.mdpi.com/2072-4292/13/8/1427⟩.
Kanniah, K.D., Najib, N.E.M. , Vu, T.T., 2016. Forest Cover Mapping in Iskandar Malaysia Using Satellite Data Int. Conf. Geomat. Geospatial Technol. (Ggt) 2016 42–4 W1 2016 71 75 doi: 10.5194/isprs-archives-XLII-4-W1-71-2016.
Kanniah, K.D., Sheikhi, A., Cracknell, A.P., Goh, H.C., Tan, K.P., Ho, C.S., Rasli, F.N., 2015. Satellite images for monitoring mangrove cover changes in a fast growing economic region in Southern Peninsular Malaysia. Remote Sens. 7 (11), 14360–14385. ://WOS:000366185200004.
Kia, M.B., Pirasteh, S., Pradhan, B., Mahmud, A.R., Sulaiman, W.N.A., Moradi, A., 2012. An artificial neural network model for flood simulation using GIS: Johor River Basin, Malaysia. Environ. Earth Sci. 67 (1), 251–264.
Kong, D., Latrubesse, E.M., Miao, C., Zhou, R., 2020. Morphological response of the Lower Yellow River to the operation of Xiaolangdi Dam, China. Geomorphology 350, 106931. https://doi.org/10.1016/j.geomorph.2019.106931.
Kudnar, N.S., 2020. GIS-based assessment of morphological and hydrological parameters of Wainganga River Basin, Central India. Model. Earth Syst. Environ. 6 (3), 1933–1950. https://doi.org/10.1007/s40808-020-00804-y.
Kumar, L., Mutanga, O., 2018. Google earth engine applications since inception: usage, trends, and potential. Remote Sens. 10 (10), 1509. ⟨https://www.mdpi.com/2072-4292/10/10/1509⟩.
Kummu, M., de Moel, H., Ward, P.J., Varis, O., 2011. How close do we live to water? A global analysis of population distance to freshwater bodies. e20578-e20578 PLoS One 6 (6). https://doi.org/10.1371/journal.pone.0020578.
Lee, W.K, Zaharuddin, N.A.b., 2015. Hydrodynamic Model for the Investigation of Environmental Flow in Johor River Estuary. In: Hassan, R., Yusoff, M., Alisibramulisi, A., Mohd Amin, N., Ismail, Z. (Eds.), InCIEC 2014. Springer, Singapore.
Legg, N., Heimburg, C., Collins, B., Olson, P., 2014. The channel migration toolbox: ArcGIS tools for measuring stream. Department of Ecology State of Washington,, Bellevue, WA, USA.
Lewandowicz, E., Flisek, P., 2020. A Method for Generating the Centerline of an Elongated Polygon on the Example of a Watercourse. ISPRS Int. J. Geo-Inf. 9 (5), 304. ⟨https://www.mdpi.com/2220-9964/9/5/304⟩.
Li, D., Lu, D., Moran, E., da Silva, R.F.B., 2020. Examining water area changes accompanying dam construction in the Madeira River in the Brazilian Amazon. Water 12 (7), 1921. ⟨https://www.mdpi.com/2073-4441/12/7/1921⟩.
Li, H., Wan, W., Fang, Y., Zhu, S., Chen, X., Liu, B., Hong, Y., 2019. A google earth engine-enabled software for efficiently generating high-quality user-ready Landsat mosaic images. Environ. Model. Softw. 112, 16–22. https://doi.org/10.1016/j.envsoft.2018.11.004.
Lin, Q., 2011. Influence of dams on river ecosystem and its countermeasures (Article). J. Water Resour. Prot. 7, 3779. https://doi.org/10.4236/jwarp.2011.31007.
Lin, X., Xu, M., Cao, C., P. Singh, R., Chen, W., Ju, H., 2018. Land-use/land-cover changes and their influence on the ecosystem in Chengdu City, China during the Period of 1992–2018. Sustainability 10 (10), 3580. ⟨https://www.mdpi.com/2071-1050/10/10/3580⟩.
Low, P.S., & Loganathan, P. (2019). *El Niño - A Review of Scientific Understanding and the Impacts of 1997/98 Event in Malaysia* (Chapter 1: General Introduction, Issue.
Luo, C., Zhang, X., Meng, X., Zhu, H., Ni, C., Chen, M., Liu, H., 2022. Regional mapping of soil organic matter content using multitemporal synthetic Landsat 8 images in Google Earth Engine. Catena 209, 105842. https://doi.org/10.1016/j.catena.2021.105842.
Magliulo, P., Valente, A., 2020. GIS-based geomorphological Map of the Calore River Floodplain Near Benevento (Southern Italy) overflooded by the 15th October 2015 event. Water 12 (1), 148. ⟨https://www.mdpi.com/2073-4441/12/1/148⟩.
Maja, M.M., Ayano, S.F., 2021. The impact of population growth on natural resources and farmers' capacity to adapt to climate change in low-income countries. Earth Syst. Environ. 5 (2), 271–283. https://doi.org/10.1007/s41748-021-00209-6.
Mountrakis, G., Im, J., Ogole, C., 2011. Support vector machines in remote sensing: a review. ISPRS J. Photogramm. Remote Sens. 66 (3), 247–259. https://doi.org/10.1016/j.isprsjprs.2010.11.001.
Nyland, K.E., Gunn, G.E., Shiklomanov, N.I., Engstrom, R.N., Streletskiy, D.A., 2018. Land cover change in the lower Yenisei River using dense stacking of landsat imagery in google earth engine. Remote Sens. 10 (8), 1226. ⟨https://www.mdpi.com/2072-4292/10/8/1226⟩.
Obaid, H., Shahid, S., 2017. Soil erosion susceptibility of Johor River basin. Water Environ. J. 31 (3), 367–374.
OECD. (2001). *OECD Environmental Outlook*. https://doi.org/doi:https://doi.org/10.1787/9789264188563-en.

Petchprayoon, P., Blanken, P.D., Ekkawatpanit, C., Hussein, K., 2010. Hydrological impacts of land use/land cover change in a large river basin in central–northern Thailand. Int. J. Climatol. 30 (13), 1917–1930. https://doi.org/10.1002/joc.2131.
Phan, T.N., Kuch, V., Lehnert, L.W., 2020. Land Cover Classification using Google Earth Engine and Random Forest Classifier—The Role of Image Composition. Remote Sens. 12 (15), 2411. ⟨https://www.mdpi.com/2072-4292/12/15/2411⟩.
Piqué, G., Batalla, R.J., Sabater, S., 2016. Hydrological characterization of dammed rivers in the NW Mediterranean region. Hydrol. Process. 30 (11), 1691–1707. https://doi.org/10.1002/hyp.10728.
Richards, D.R., Belcher, R.N., 2020. Global changes in urban vegetation cover. Remote Sens. 12 (1), 23. ⟨https://www.mdpi.com/2072-4292/12/1/23⟩.
Roy, D.P., Ju, J., Kline, K., Scaramuzza, P.L., Kovalskyy, V., Hansen, M., Loveland, T.R., Vermote, E., Zhang, C., 2010. Web-enabled Landsat Data (WELD): Landsat ETM+ composited mosaics of the conterminous United States. Remote Sens. Environ. 114 (1), 35–49.
Roy, P., Roy, A., 2010. Land use and land cover change in India: aremote sensing & GIS prespective. J. Indian Inst. Sci. 90 (4), 489–502.
Sabater, S., Bregoli, F., Acuña, V., Barceló, D., Elosegi, A., Ginebreda, A., Marcé, R., Muñoz, I., Sabater-Liesa, L., Ferreira, V., 2018. Effects of human-driven water stress on river ecosystems: a meta-analysis. Sci. Rep. 8 (1), 11462. https://doi.org/10.1038/s41598-018-29807-7.
Saudi, A.S.M., Juahir, H., Azid, A., Azaman, F., 2015. Flood risk index assessment in Johor River Basin. Malays. J. Anal. Sci. 19 (5), 991–1000.
Sejati, A.W., Buchori, I., Kurniawati, S., Brana, Y.C., Fariha, T.I., 2020. Quantifying the impact of industrialization on blue carbon storage in the coastal area of Metropolitan Semarang, Indonesia. Appl. Geogr. 124, 102319 https://doi.org/10.1016/j.apgeog.2020.102319.
Shaharum, N.S.N., Shafri, H.Z.M., Ghani, W.A.W.A.K., Samsatli, S., Al-Habshi, M.M.A., Yusuf, B., 2020. Oil palm mapping over Peninsular Malaysia using Google Earth Engine and machine learning algorithms. Remote Sens. Appl.: Soc. Environ. 17, 100287 https://doi.org/10.1016/j.rsase.2020.100287.
Sheykhmousa, M., Mahdianpari, M., Ghanbari, H., Mohammadimanesh, F., Ghamisi, P., Homayouni, S., 2020. Support vector machine vs. random forest for remote sensing image classification: a meta-analysis and systematic review. IEEE J. Sel. Top. Appl. Earth Obs. Remote Sens.
Sinha, M., Mukhopadhyay, M., Mitra, P., Bagchi, M., Karamkar, H., 1996. Impact of Farakka barrage on the hydrology and fishery of Hoogly estuary. Estuaries 19 (3), 710–722.
Sinha, R.K., Eldho, T.I., Subimal, G., 2020. Assessing the impacts of land use/land cover and climate change on surface runoff of a humid tropical river basin in Western Ghats, India. Int. J. River Basin Manag. 1–12. https://doi.org/10.1080/15715124.2020.1809434.
Song, X.-P., Hansen, M.C., Stehman, S.V., Potapov, P.V., Tyukavina, A., Vermote, E.F., Townshend, J.R., 2018. Global land change from 1982 to 2016. Nature 560 (7720), 639–643. https://doi.org/10.1038/s41586-018-0411-9.
Souza-Filho, P.W.M., de Souza, E.B., Silva Júnior, R.O., Nascimento, W.R., Versiani de Mendonça, B.R., Guimarães, J.T.F., Dall'Agnol, R., Siqueira, J.O., 2016. Four decades of land-cover, land-use and hydroclimatology changes in the Itacaiúnas River watershed, southeastern Amazon. J. Environ. Manag. 167, 175–184. https://doi.org/10.1016/j.jenvman.2015.11.039.
Spada, D., Molinari, P., Bertoldi, W., Vitti, A., Zolezzi, G., 2018. Multi-temporal image analysis for fluvial morphological characterization with application to Albanian rivers. ISPRS Int. J. Geo-Inf. 7 (8), 314. ⟨https://www.mdpi.com/2220-9964/7/8/314⟩.
Sun, X., Li, G., Wang, J., Wang, M., 2021. Quantifying the land use and land cover changes in the Yellow River Basin while accounting for data errors based on globeland30 maps. Land 10 (1), 31. ⟨https://www.mdpi.com/2073-445X/10/1/31⟩.
Surian, N., Rinaldi, M., 2003. Morphological response to river engineering and management in alluvial channels in Italy. Geomorphology 50 (4), 307–326. https://doi.org/10.1016/S0169-555X(02)00219-2.
Tamiminia, H., Salehi, B., Mahdianpari, M., Quackenbush, L., Adeli, S., Brisco, B., 2020. Google Earth Engine for geo-big data applications: a meta-analysis and systematic review. ISPRS J. Photogramm. Remote Sens. 164, 152–170. https://doi.org/10.1016/j.isprsjprs.2020.04.001.
Tan, K.C., Lim, H.S., MatJafri, M.Z., Abdullah, K., 2010. Landsat data to evaluate urban expansion and determine land use/land cover changes in Penang Island, Malaysia. Environ. Earth Sci. 60 (7), 1509–1521. https://doi.org/10.1007/s12665-009-0286-z.
Tan, M.L., Chua, V.P., Li, C., Brindha, K., 2019a. Spatiotemporal analysis of hydro-meteorological drought in the Johor River Basin, Malaysia. Theor. Appl. Climatol. 135 (3–4), 825–837. https://doi.org/10.1007/s00704-018-2409-5.
Tan, M.L., Ibrahim, A.L., Yusop, Z., Duan, Z., Ling, L., 2015. Impacts of land-use and climate variability on hydrological components in the Johor River basin, Malaysia. Hydrol. Sci. J. 60 (5), 873–889. https://doi.org/10.1080/02626667.2014.967246.
Tan, M.L., Juneng, L., Tangang, F.T., Chan, N.W., Ngai, S.T., 2019b. Future hydro-meteorological drought of the Johor River Basin, Malaysia, based on CORDEX-SEA projections. Hydrol. Sci. J. -J. Des. Sci. Hydrol. 64 (8), 921–933. https://doi.org/10.1080/02626667.2019.1612901.
Tankpa, V., Wang, L., Atanga, R.A., Awotwi, A., Guo, X., 2020. Evidence and impact of map error on land use and land cover dynamics in Ashi River watershed using intensity analysis. PLoS One 15 (2), e0229298. https://doi.org/10.1371/journal.pone.0229298.
Wahap, N.A., Shafri, H.Z.M., 2020. Utilization of google earth engine (GEE) for land cover monitoring over Klang Valley, Malaysia. IOP Conf. Ser.: Earth Environ. Sci. 540 (1), 012003 https://doi.org/10.1088/1755-1315/540/1/012003.
Wang, F., Ge, Q., Yu, Q., Wang, H., Xu, X., 2017. Impacts of land-use and land-cover changes on river runoff in Yellow River basin for period of 1956–2012. Chin. Geogr. Sci. 27 (1), 13–24. https://doi.org/10.1007/s11769-017-0843-3.
Wang, X., Su, F., Zhang, J., Cheng, F., Hu, W., Ding, Z., 2019. Construction land sprawl and reclamation in the Johor River Estuary of Malaysia since 1973. Ocean Coast. Manag. 171, 87–95.
Winkler, K., Fuchs, R., Rounsevell, M., Herold, M., 2021. Global land use changes are four times greater than previously estimated. Nat. Commun. 12 (1), 2501. https://doi.org/10.1038/s41467-021-22702-2.
Wolde, Z., Wei, W., Likessa, D., Omari, R., Ketema, H., 2021. Understanding the impact of land use and land cover change on water-energy-food nexus in the Gidabo Watershed, East African Rift Valley. Nat. Resour. Res. 30 (3), 2687–2702. https://doi.org/10.1007/s11053-021-09819-3.
Woldemichael, A.T., Hossain, F., Pielke Sr., R., Beltrán-Przekurat, A., 2012. Understanding the impact of dam-triggered land use/land cover change on the modification of extreme precipitation. Water Resour. Res. 48 (9) https://doi.org/10.1029/2011WR011684.
Xie, S., Liu, L., Zhang, X., Yang, J., Chen, X., Gao, Y., 2019. Automatic land-cover mapping using landsat time-series data based on google earth engine. Remote Sens. 11 (24), 3023. ⟨https://www.mdpi.com/2072-4292/11/24/3023⟩.
Yang, Y., Liu, Y., Xu, D., Zhang, S., 2017. Use of intensity analysis to measure land use changes from 1932 to 2005 in Zhenlai County, Northeast China. Chin. Geogr. Sci. 27 (3), 441–455. https://doi.org/10.1007/s11769-017-0876-8.
Yousefi, S., Moradi, H.R., Keesstra, S., Pourghasemi, H.R., Navratil, O., Hooke, J., 2019. Effects of urbanization on river morphology of the Talar River, Mazandarn Province, Iran. Geocarto Int. 34 (3), 276–292. https://doi.org/10.1080/10106049.2017.1386722.
Yousefi, S., Pourghasemi, H.R., Hooke, J., Navratil, O., Kidová, A., 2016. Changes in morphometric meander parameters identified on the Karoon River, Iran, using remote sensing data. Geomorphology 271, 55–64. https://doi.org/10.1016/j.geomorph.2016.07.034.
Zagajewski, B., Kluczek, M., Raczko, E., Njegovec, A., Dabija, A., Kycko, M., 2021. Comparison of random forest, support vector machines, and neural networks for post-disaster forest species mapping of the krkonose/karkonosze transboundary biosphere reserve. Remote Sens. 13 (13). ://WOS:000671164200001.
Zhao, S., Peng, C., Jiang, H., Tian, D., Lei, X., Zhou, X., 2006. Land use change in Asia and the ecological consequences. Ecol. Res. 21 (6), 890–896. https://doi.org/10.1007/s11284-006-0048-2.
Zhou, P., Huang, J., Pontius, R.G., Hong, H., 2014. Land classification and change intensity analysis in a coastal watershed of Southeast China. Sensors 14 (7), 11640–11658. ⟨https://www.mdpi.com/1424-8220/14/7/11640⟩.
Zope, P.E., Eldho, T.I., Jothiprakash, V., 2017. Hydrological impacts of land use–land cover change and detention basins on urban flood hazard: a case study of Poisar River basin, Mumbai, India. Nat. Hazard. 87 (3), 1267–1283. https://doi.org/10.1007/s11069-017-2816-4.